1-1-2019

Evaluating the effects of water influx on the Mississippi sound: current vs. Historical relationships

Jarett Lee Bell

EVALUATING THE EFFECTS OF WATER INFLUX ON THE MISSISSIPPI SOUND: CURRENT VS. HISTORICAL RELATIONSHIPS

A Thesis Proposal presented in partial fulfillment of requirements for the degree of Master of Science in the Department of Geology and Geological Engineering the University of Mississippi

by

Jarett Bell

August 2019

ABSTRACT

This research investigated the influence of the opening of the Bonnet Carre Spillway and other fresh water inputs on the Mississippi Sound. The Bonnet Carre Spillway was completed in 1931 and was constructed to protect New Orleans whenever the Mississippi River is at flood stage. The spillway drains into Lake Pontchartrain, a brackish-water lagoon north of New Orleans, which then drains into Lake Borgne and subsequently into the Mississippi Sound. The inflow of water from the spillway changes the water chemistry of all receiving water bodies and impacts the waters of the Mississippi Gulf Coast. We collected in-situ temperature, specific conductance, and dissolved oxygen data for the Spring of 2018 opening event, and used these data in addition to remotely sensed data for tracking the movement of river water plume/plumes through the coastal waters. Remote sensing data was collected from Landsat and Sentinel 2 platforms, and were all processed to track freshwater plumes where possible. Specific conductance and temperature both displayed the effect of the Bonnet Carre Spillway within 13 and 18 days, respectively, while dissolved oxygen did not show a clear pattern of impact. The three remote sensing analyses completed were: Sentinel 2 single band and multispectral analysis, Landsat 8 multispectral analysis, and Landsat thermal analysis. All of which were successful at identifying the Bonnet Carre Spillway plume, near the source influx. Identification of the Bonnet Carre Spillway plume within the Mississippi sound was not possible due to water column mixing beyond the source influx. Lastly, features present in our study area were the result of a combination of Pearl River plumes and increased sediment suspension from Lake Pontchartrain flushing out through the Rigolets channel.

DEDICATION

This thesis is dedicated to friends, family, and colleagues who helped and aided me in my journey throughout my undergraduate and graduate program.

LIST OF ABBREVIATIONS AND SYMBOLS

BOA	Bottom of Atmosphere
DO	Dissolved Oxygen
ESA	European Space Agency
GoM	Gulf of Mexico
ka	kiloyear (thousand years)
LIS	Laurentide Ice Sheet
MBRACE	Mississippi-Based RESTORE Act Center of Excellence
OOS	Ocean Observing Stations
SC	Specific Conductance

ACKNOWLEDGMENTS

I express my deepest appreciation to my advisor, Dr. Greg Easson and my committee members: Dr. Louis Zachos, and Dr. Lance Yarbrough. I am thankful for the opportunity that Dr. Greg Easson and the Mississippi-Based RESTORE Act Center of Excellence have provided to complete my master's research while investigating freshwater influx on the Mississippi Sound.

TABLE OF CONTENTS

ABSTRACT II

DEDICATION III

LIST OF ABBREVIATIONS AND SYMBOLS IV

ACKNOWLEDGMENTS V

TABLE OF CONTENTS VI

LIST OF TABLES VIII

LIST OF FIGURES IX

I. INTRODUCTION 1

II. BACKGROUND 3

1 Study Area 3

2 Gulf of Mexico and Mississippi Sound Overview 4

3 Pleistocene Glaciation (Wisconsin) 6

4 Hydrogeologic Overview 8

III. METHODS 11

1 Equipment 11

2 Deployment 12

3 Landsat/Sentinel 2 Imagery Collection 14

4 Landsat Scene Clipping 16

5 Landsat Scene Land Masking 17

6 Landsat Surface Water Temperature 18

7 Post Model & Single Band/Multispectral Scene Processing 22

IV RESULTS & DISCUSSION 24

1 2018 Bonnet Carre Study Data 24

2 Data Validation 28

3 Sentinel 2 Multispectral and Single Band Data 32

4 Landsat 8 Multispectral Visual Imagery 39

5 Thermally Processed Landsat Data 44

V CONCLUSIONS 49

REFERENCES 51

APPENDIX 55

VITA 59

LIST OF TABLES

Table 1: Average yearly discharge amounts of rivers into the Mississippi Sound (Eleuterius, 1978) 10

Table 2: Landsat/Sentinel 2 scene collection dates 14

Table 3: Sentinel 2 multispectral and single band analysis imagery collection dates 32

Table 4: Thermal analysis sampling locations average temperature (°C) 44

LIST OF FIGURES

Figure 1: Water quality data collection study area....3

Figure 2: Laurentide ice sheet extent and available dates (Prest, 1984) 7

Figure 3: Louisiana lakes and passes overview *(Sikora and Kjerfve, 1985)* 8

Figure 4: Mississippi Sound influx sources: rivers (major and minor)....9

Figure 5: OOS with biosensor rack and abiotic sensors....11

Figure 6: Launch of the OOS....13

Figure 7: Clipping model....16

Figure 8: Land masking model 17

Figure 9: Landsat 4-5 land surface temperature model....18

Figure 10: Landsat 7 land surface temperature model 18

Figure 11: Landsat 8 land surface temperature model 19

Figure 12: Specific conductance (µS/cm) for the 2018 Bonnet Carre collection event....24

Figure 13: Dissolved oxygen (mg/L) for the 2018 Bonnet Carre collection event....25

Figure 14: Temperature (°F) for the 2018 Bonnet Carre collection event 25

Figure 15: 2019 Sentinel 2 plume extent proxy image for 2018 Bonnet Carre Spillway opening 27

Figure 16: USGS Merrill Shell sensor station 29

Figure 17: Specific Conductance (µS/cm) comparison between USGS Merrill Shell station data and 2018 Bonnet Carre Study data....30

Figure 18: Temperature (°C) comparison between USGS Merrill Shell station data and 2018 Bonnet Carre Study data 31
Figure 19: Multispectral imagery sampling locations 32
Figure 20: Multispectral Response Curves for the 2016 closed and opened Bonnet Carre Spillway 33
Figure 21: Sentinel 2 image showing Bonnet Carre Spillway plume extent and multispectral sampling locations 34
Figure 22: Single band spectral analysis sampling locations 35
Figure 23: Sentinel 2 Band 1 spectral response curves for the 2016 and 2018 Bonnet Carre Spillway opening events 36
Figure 24: 2016 Sentinel 2 image showing Bonnet Carre Spillway plume extent and Sentinel 2 band 1 sampling locations 37
Figure 25: 2018 Sentinel 2 image showing Bonnet Carre Spillway plume extent and Sentinel 2 band 1 sampling locations 38
Figure 26: February 10, 2016 Multispectral image with Bonnet Carre Spillway closed .. 39
Figure 27: January 17, 2016 Multispectral image with Bonnet Carre Spillway opened ... 40
Figure 28: March 3, 2018 Multispectral image with Bonnet Carre Spillway closed 41
Figure 29: March 6, 2019 Multispectral image with Bonnet Carre Spillway open 42
Figure 30: March 22, 2019 Multispectral image with Bonnet Carre Spillway open 43
Figure 31: February 26, 2016 Surface water temperature map: Bonnet Carre Spillway closed 45

Figure 32: January 17, 2016 Surface water temperature map: Bonnet Carre Spillway opened....46
Figure 33: March 3, 2018 Surface water temperature map: Bonnet Carre Spillway closed 46
Figure 34: March 6, 2019 Surface water temperature map: Bonnet Carre Spillway opened 47
Figure 35a: Specific Conductance with Precipitation....56
Figure 36a: Dissolved Oxygen with Precipitation....57
Figure 37a: Temperature with Precipitation....58

I. INTRODUCTION

The Bonnet Carre Spillway was constructed in response to the flood of 1927 and was completed in 1931. The spillway drains flood water from the Mississippi River into Lake Pontchartrain, a 1630 km^2 brackish-water lagoon north of New Orleans (Lane et al., 2001). Lake Pontchartrain then drains into Lake Borgne which subsequently drains into Mississippi Sound. The water flowing from the opening of the spillway changes the water chemistry and introduces a large sediment load into these receiving bodies.

The Mississippi Gulf Coast oyster reefs are an important coastal ecosystem providing significant economic resources for many communities along the Mississippi Gulf Coast. However, in recent years the Mississippi Gulf Coast oyster reefs have been on the decline, with an approximate 15-fold decline over the past decade. As a result of this decline the state of Mississippi has started an oyster reef restoration plan with a goal of sustainable oyster reefs and future production. The Mississippi-Based RESTORE ACT Center of Excellence (MBRACE) and its partners: University of Sothern Mississippi, Jackson State University, University of Mississippi, and Mississippi State University are supporting this goal through MBRACE's Core Research Program Topic Area: "*Understanding oyster reefs and their sustainability*".

The goal of the University of Mississippi's portion of that project is to identify differences in abiotic and biotic stressors at current and historic oyster reef sites. These data will provide a better understanding of oyster reef health and inform management about the best places and practices to improve oyster reef restoration strategies. The goal of this thesis is to

evaluate water quality parameters and use remotely sensed data to track influxes of freshwater into the Mississippi sound, including the opening of the Bonnet Carre Spillway on the Mississippi Sound.

The data collection used to assess the influence of influx waters from the Bonnet Carre Spillway on the Mississippi Sound and oyster reefs was conducted using water ocean observing stations (OOS) which carry sensors to measure water quality parameters and biotic oyster sensors. Satellite imagery was also used to assess the temporal, spatial, and spectral relationship between the water quality parameters. Water quality parameters recorded were temperature, conductivity, turbidity, and dissolved oxygen. The biotic parameters are determined using "biosensors" (oysters) which are placed along with the abiotic sensors.

II. BACKGROUND

1 Study Area

The study area for this thesis spans from the Bonnet Carre Spillway at the western edge of Lake Pontchartrain, Louisiana to Pass Christian, Mississippi. Water quality data was collected from a set of 11 sensors positioned in a line from the western most tip of Henderson Point in Pass Christian Mississippi to the western most tip of Cat Island. The sensors crossed Mississippi public fishing harvest zones of Area II "A", "F", "G", and "I" (Figure 1).

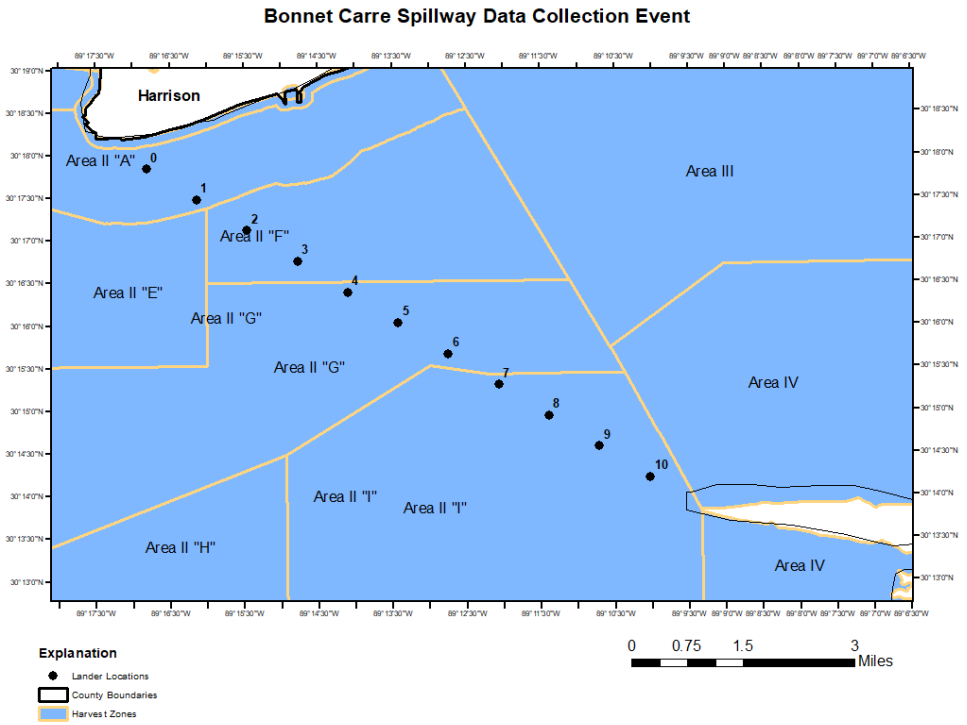

Figure 1: Water quality data collection study area

2 *Gulf of Mexico and Mississippi Sound Overview*

The Gulf of Mexico (GoM) basin is the largest semi enclosed depositional basin in North America. Sediments from the Mississippi River have built a thick sequence of inter-fingering deltaic, nearshore coastal brackish water, and marine sediments during the Middle to late Mesozoic and Cenozoic (Coleman et al., 1991). Quaternary deposits within the GoM basin are estimated to have accumulated as much as 3000 to 3600 meters of sediment to the present shelf in offshore Louisiana and Texas, and the vicinity of the present Mississippi Fan, respectively (Coleman et al., 1991). However, accumulation estimates for the western and southern rim of the GoM basin are unknown, as little research has been completed in the area.

The morphology and sedimentation of the GoM throughout the Quaternary is the direct result of changes in climate, vegetation, drainage patterns, discharge characteristics, and sea level; with the largest influence being climatic changes, which caused major fluctuations of sea level throughout the Quaternary (Coleman et al., 1991). Sea level lowering was the direct result of expanding glaciers, while sea level rise was due to retreating glaciers. The last major sea level low stand event occurred approximately 18,000 years ago, during the Wisconsin Glaciation, with sea level change estimates ranging from 76 to 85 meters (Denton and Terence, 1981; Coleman et al., 1991). Expanding glaciers resulted in exposure of the continental shelf, lowered base levels of streams, caused entrenchment of rivers, and deposition and/or modification of subaerial/aqueous Quaternary sediment. Retreating glaciers resulted in submerged coastal plains, aggrading river valleys, and deposition and/or modification of subaerial/aqueous Quaternary sediment.

The Pleistocene and Holocene sediments associated with sea level rise and fall display a high variability/complexity with regard to process controls, facies, and characterization

depending on location; with the subaerial deposits of the east and south GoM being most complex. These sediments are characterized by predominantly carbonate deposition, merging with quartz-rich sands of the barrier island-lagoon complex of Alabama and Mississippi (Coleman et al., 1991). Facies patterns tend to parallel the Florida coastline and display carbonates mixed with quartz sand nearshore grading into carbonate mudstones near the shelf edge. The west Florida shelf then merges into the relic sand sheet of peninsular Florida, Alabama, and Mississippi (Coleman et al., 1991). The central northern GoM is characterized as being a deviation of modern Mississippi River plain and marginal chenier plain sediments, with complex sediment facies; while the northern continental slope of the GoM contains shale and salt diapirs which form topographic basins and highs. These basins are covered with fine-grained pelagic and hemiplegic sediments, while topographic highs are primarily carbonate-rich sediments (Coleman et al., 1991). The Texas and north eastern Mexican coast possesses barrier islands and lagoons on the coastal plain, while the subaqueous broad shelf has little topographic relief and consists mostly of relic sediments (Coleman et al., 1991).

Coleman et al. (1991), divide beaches and islands in the north GoM into three categories: (1) quartz-rich barrier islands of peninsular Florida, Alabama, and Mississippi, (2) the chenier plain of western Louisiana, and (3) the barrier island complex off Texas and northeastern Mexico. The Mississippi-Alabama-Florida barrier islands extend from peninsular Florida to the Mississippi Delta and began forming approximately around 5000 to 6000 years ago during a period of low sea level stability (Coleman et al., 1991). The islands are Holocene to Wisconsinan-age depending on connection to the mainland, and in some cases cause the Holocene beach deposits to be welded to the Wisconsinan-age coastal beach and eolian deposits (Otvos, 1984; Coleman et al., 1991). The major characteristics of all these barrier islands is that

they are composed of clean, fine to medium grained quartz sand, sometimes reaching 99% quartz. Heavy mineral analysis of the sand indicates that the source is in the Appalachians and was delivered along small streams originating from the southern end of the mountains and extended across the continental shelf during lower sea levels, which became entrenched and delivered small amounts of bedload to the self-edge. During rising sea level, fines were winnowed out of the sediments by wave processes which concentrated heavy minerals and quartz. Presently, little sediment is supplied to these barrier islands, except for headland area erosion and lateral migration.

3 Pleistocene Glaciation (Wisconsin)

The greatest influence on the formation of the current geomorphology of the GoM was the late Pleistocene glaciation and resultant deglaciation. The Pleistocene glaciation is also known as the Late Wisconsin Glaciation and resulted in the Laurentide Ice Sheet (LIS). The LIS covered most of Canada and part of the northern United States (Andrews, 1987)(Figure 2). The calculated maximum and minimum estimates for global sea level change of the LIS was between 76 and 85 meters respectively (Denton and Terence, 1981). Generalized deglaciation hypothesis of the LIS involved at least two catastrophic collapse events, with the first collapse occurring approximately at 8 ka near the Hudson Strait and Hudson Bay which resulted in rapid deglaciation (Falconer et al., 1965; Falconer and Andrews, 1969; Prest, 1970). The second

collapse occurred at 6.7 ka in the Foxe Basin north of Hudson Bay (Blake, W., 1966; Andrews, 1970)(Figure 2).

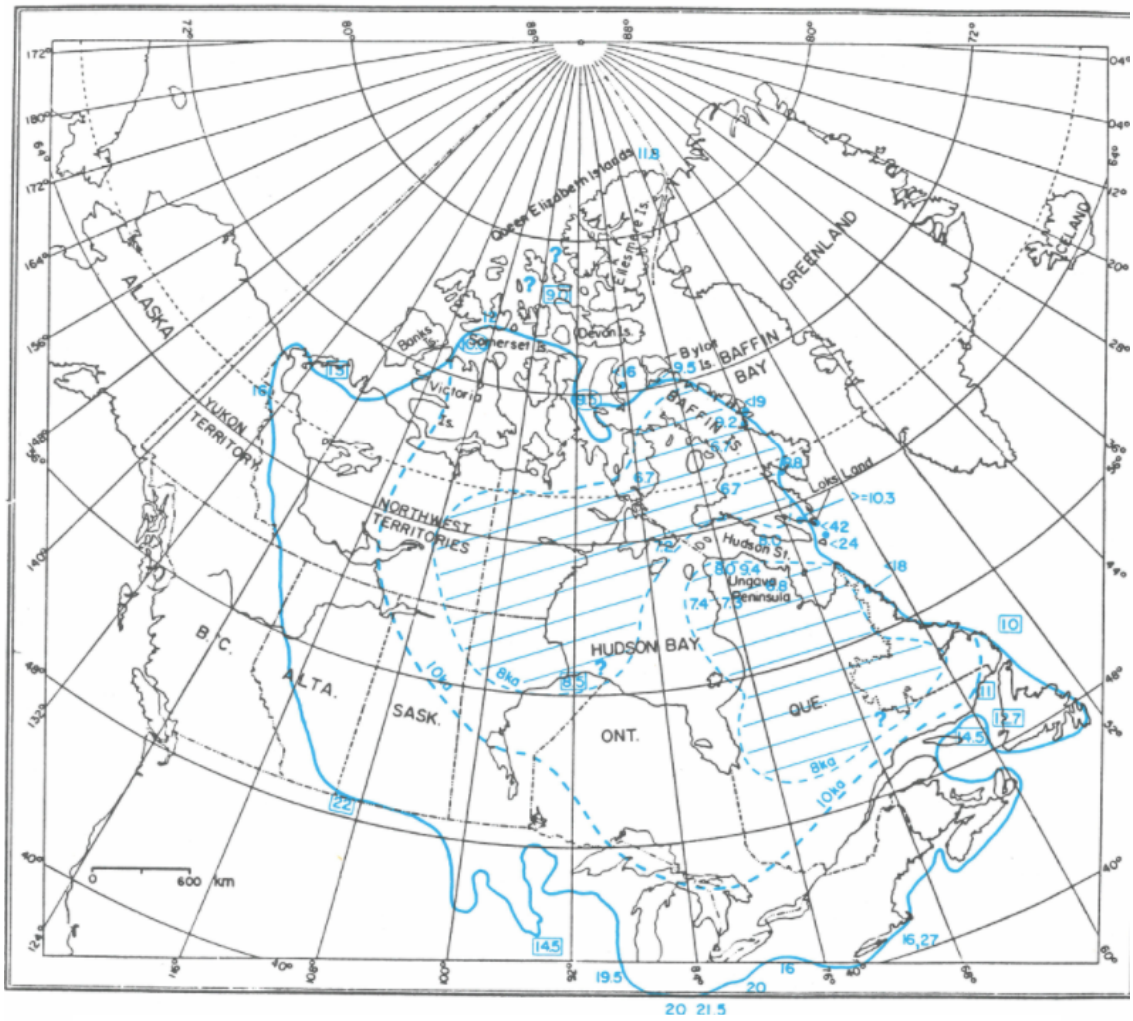

Figure 2: Laurentide ice sheet extent and available dates (Prest, 1984)

The deglaciation of the LIS can be attributed to both global influences and regional controls. At the global level, melting of the southern margins would cause a global rise in sea level and would result in destabilization and rapid retreat of south and west margins. However, the north and east margins, which were dominated by regional processes, reaction to sea level change would stabilize margin retreat. Lastly, Michelson et al.(1983), proposed that the southern margin of the Laurentide glaciation re-advanced, despite the continued deglaciation at 1 ka intervals from 21–14.8ka.

4 Hydrogeologic Overview

Lake Pontchartrain formed approximately 500 years ago as a shallow bay during the late stages of the Wisconsin post-glacial sea level rise and was formed by the Crocodile and the St. Bernard Mississippi River delta building periods (Sikora and Kjerfve, 1985). Lake Pontchartrain has a diurnal tide with a mean range of 11 cm and an estimated flushing time of 60 days (Sikora and Kjerfve, 1985). The water column is generally well mixed and has weak stratification near the two natural tidal passes (the Rigolets opening into Lake Borgne/Western Mississippi Sound, Chef Menteur opening into Lake Borgne, and the Inner Harbor Navigation Canal) located on the southeast side of Lake Pontchartrain which opens into the Intracoastal Waterway (Sikora and Kjerfve, 1985)(Figure 3).

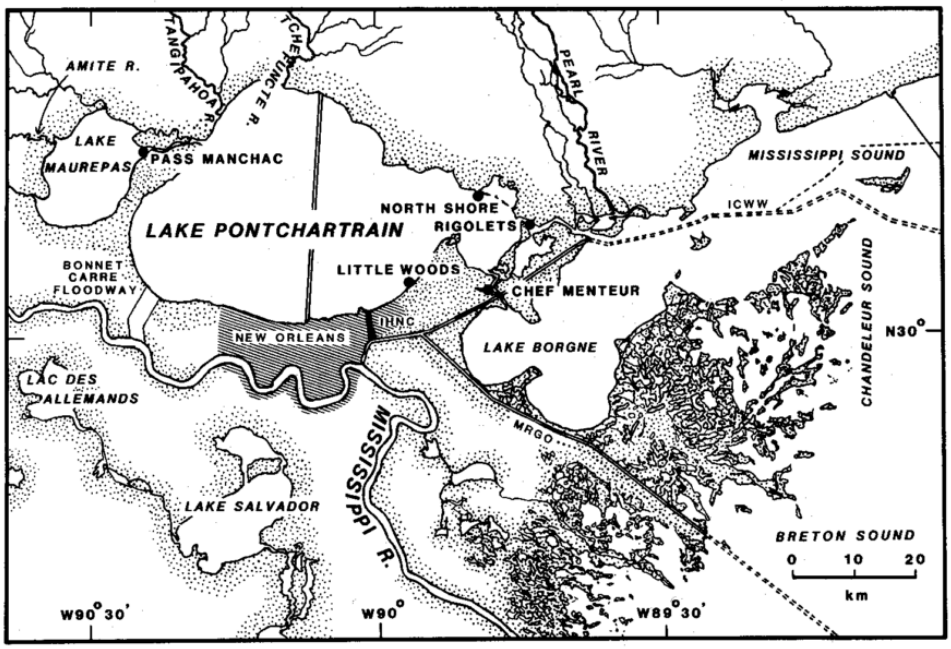

Figure 3: Louisiana lakes and passes overview *(Sikora and Kjerfve, 1985)*

The Mississippi Sound is a coastal, partly enclosed estuary with a mean depth of 3 meters at mid-tide (Chigbu et al., 2004). Within the estuary, water from the GoM mixes with 6 rivers, and several bayous. The four minor rivers, accounting for 10% of freshwater influx into the Mississippi Sound, are the Biloxi, Tchouticabouffa, Jourdan, and Wolf, while the two major rivers, accounting for 90% of discharge into the Mississippi Sound are the Pearl and Pascagoula Rivers (Eleuterius, 1978)(Figure 4)(Table 1). The largest influx of freshwater into the Mississippi Sound comes from the Pearl River which is roughly 789 km long and drains an area

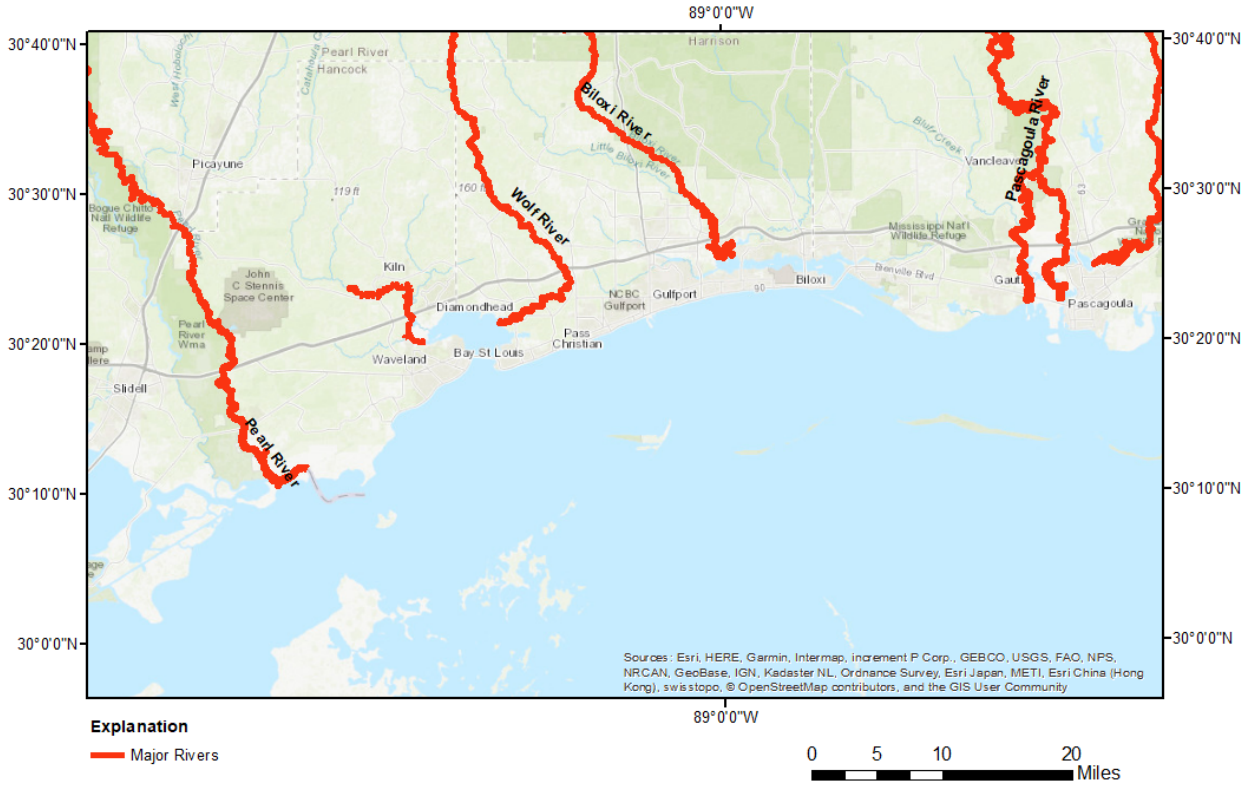

Figure 4: Mississippi Sound influx sources: rivers (major and minor)

of approximately 23,000 km^2 (Chigbu et al., 2004). The Mississippi Sound is characterized as partially or well mixed due to tidal action and winds while tides are diurnal with an average range of 0.57 meters (Eleuterius, 1978). Water quality parameters collected over an 11 year period, from 1990 to 2001, recorded parameters of temperature and salinity of the Mississippi

Sound on a weekly/every other day schedule which show an average temperature of 16.16° Celsius and an average salinity of 13.70 parts per thousand (ppt) (Chigbu et al., 2004).

Table 1: Average yearly discharge amounts of rivers into the Mississippi Sound (Eleuterius, 1978)

River	**Discharge (m^3/s)**
Biloxi	13.97
Tchouticabouffa	12.36
Jourdan	23.47
Wolf River	19.98
Pearl	327.72
Pascagoula	378.35

III. METHODS

1 Equipment

Data collection for this study was completed using 11 OOS carrying temperature and light, conductivity, and dissolved oxygen sensors. The OOS were constructed from aluminum to house both the instruments and biosensors (Figure 5). The OOS also have a tire placed below to ensure the platforms stay above the fine-grained sediment on the seafloor during

Figure 5: OOS with biosensor rack and abiotic sensors

deployment. An additional safety measure implemented, to aid in reduction of instrument loss, was the use of galvanic releases, which attached buoys to the platform to enable the buoy to be hidden until approximately 1 week after deployment. Biosensors were also used in the form of oysters; however, collected data is not relevant to this study. Biosensors were contained inside of a milk crate divided into 4 levels. The abiotic sensors were placed inside the platforms as well to ensure safety from physical elements and were held in placed by cable ties. The sensors used were manufactured by ONSET, and supplied via MicroDAQ. The temperature and light sensor was an ONSET HOBO UA-002-64 model which recorded temperature (°C) and light (lux) every five minutes. The conductivity sensor was an ONSET HOBO U24-002-C model which recorded high and low range conductivity (µS/cm) and temperature (°F) every five minutes. The dissolved oxygen sensor was an ONSET HOBO U26-001 model and recorded dissolved oxygen concentration (mg/L) and temperature (°F) every five minutes. The sensors were activated and managed using the HOBO Waterproof Shuttle as an optic station with a provided Microsoft Surface Tablet and HOBOware software package.

2 Deployment

The 11 OOS were deployed for two data collection events designed to capture the influx of fresh water from the opening of the Bonnet Carre Spillway into the Mississippi Sound. The two events were from March 14, 2018 through April 1, 2018 and April 1, 2018 through April 25, 2018. The locations were chosen in an attempt to ensure complete coverage of water influx from the Bonnet Carre Spillway into the Mississippi Sound. The OOS spacing was approximately 0.4 kilometers, and the average depth of each OOS was 4.6 meters. For each event the sensors were activated, using a delayed start of 5:00 p.m. the same day, before securing them onto the OOS. Once the sensors were secured to the OOS the galvanic releases were secured to the buoy and

OOS. Deployment of the OOS was completed by lowering them onto the seafloor from the side of the boat using a loose rope passed between the OOS (Figure 6). Hand lowering of the OOS was completed to ensure an upright OOS position. Recovery of the OOS, on April 1, 2018, involved pulling them from the water, and transporting the OOS back to the dock for relaunch operations. Once at the dock the sensors were removed, offloaded, cleaned (if necessary), and re-launched using the same method described above. The galvanic releases were also replaced, and the OOS were redeployed at the locations for the period of April 1 through April 25. The recovery on April 25 follows the same method used above, however the instruments were stopped and offloaded, then transported back to the University of Mississippi. Lastly, once at the University of Mississippi the sensor data was processed using HOBOware Pro software and the built-in conductivity assistant that calculates specific conductance from conductance using a linear compensation at 2.1%/°C for NaCL, and

Figure 6: Launch of the OOS

the factory calibration. Once converted the data was exported into Excel files, and subset into one-hour sampling intervals.

3 Landsat/Sentinel 2 Imagery Collection

Imagery data covering the study area were collected for March 2018 and for selected previous openings of the Bonnet Carre Spillway (Table 2). The two scenes collected were Mississippi 21/39 (Path/Row), and Louisiana 22/39 for Landsat imagery. The search coordinates for Sentinel imagery were Mississippi: 30.3475°, -89.31667° (decimal degrees) and Louisiana: 30.20861°, -90.15583°. Preprocessing of the Sentinel 2 data was necessary to take the imagery from a level 1C product to a 2A product which yields the bottom-of-atmosphere (BOA) values. This process involved using the program Sen2Cor (version 02.05.05) provided by the European Space Agency (ESA). The imagery selected for download were cloud free.

Table 2: Landsat/Sentinel 2 scene collection dates

Mississippi	**Date**	**Landsat 8**	**Landsat 7**	**Landsat 4-5**	**Sentinel 2**
2019	03/06/19	X			
	03/22/19	X			
2018	03/04/16				X
	03/12/18	X			
	03/14/18				X
	04/29/18	X			
2016	01/04/18				X
	01/17/18				X

	01/18/16	X			
	02/11/16		X		
	02/19/16	X			
	02/27/16		X		
2011	05/04/11		X		
	05/20/11		X		
	05/28/11			X	
	06/05/11		X		
	06/13/11			X	
	06/29/11			X	
2008	04/17/08			X	
	05/11/08		X		
1997	04/03/97			X	

Louisiana	**Date**	**Landsat 8**	**Landsat 7**	**Landsat 4-5**	**Sentinel 2**
2018	03/3/18	X			
	03/07/18				X
	03/12/18				X
	04/20/18	X			
2016	01/04/16				X
	01/17/16		X		X
	02/10/16	X			

	02/26/16	X			
2011	05/11/11		X		
	05/27/11		X		
	06/04/11			X	
	06/12/11		X		
	06/28/11		X		
2008	04/08/08			X	
	04/24/08			X	
	05/10/08			X	
1997	03/09/97			X	

4 Landsat Scene Clipping

All Landsat scenes collected were clipped to remove the no-data border, using a model generated in ArcMap ModelBuilder (Figure 7). The model consisted of an iterator, which generates a list of

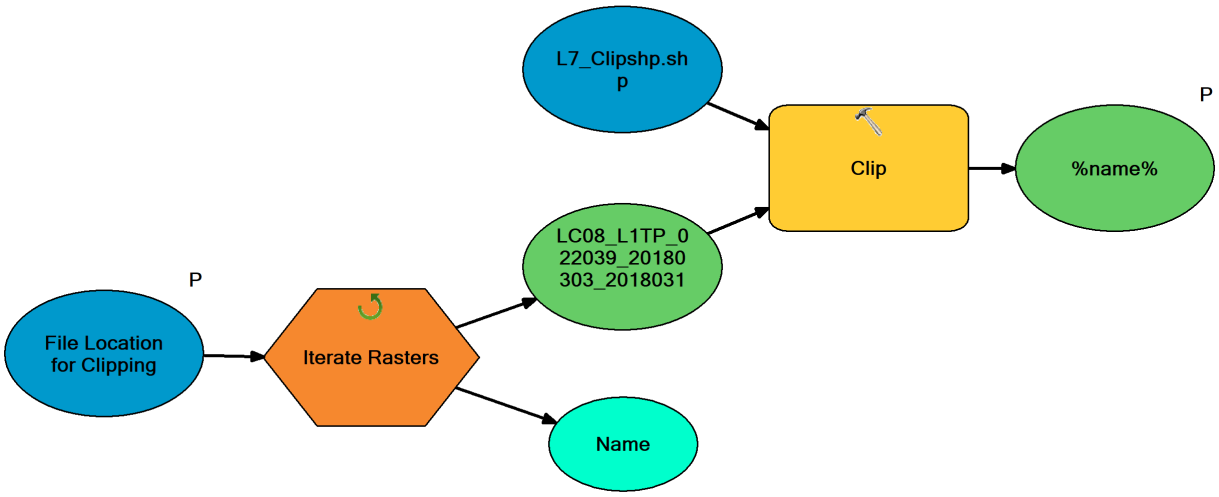

Figure 7: Clipping model

raster files for a file location, and a clipping function that clips the raster files to a specified shape and then outputs them with the same filename. Two sets of three models were used due to the two differing Landsat scenes for Mississippi 21/39 (WRS Path/Row), and Louisiana 22/39. Three model iterations were needed due to having Landsat 4-5, Landsat 7, and Landsat 8 scenes, all of which have a different collection angle and result in differing clipping shape.

5 *Landsat Scene Land Masking*

All Landsat scenes collected above were land masked to limit the influence of terrestrial land cover. The mask provided more accurate calculations of water surface temperature, and multispectral analysis. The land mask was created using a model generated in ArcMap ModelBuilder (Figure 8). The model consisted of a Landsat near infrared (NIR) band input which processed using an Iso-Cluster Unsupervised Classification, with two classes. These two classes were reclassified so that land features were classified as 0 and water features as 1. This reclassified raster was then used in a nested model

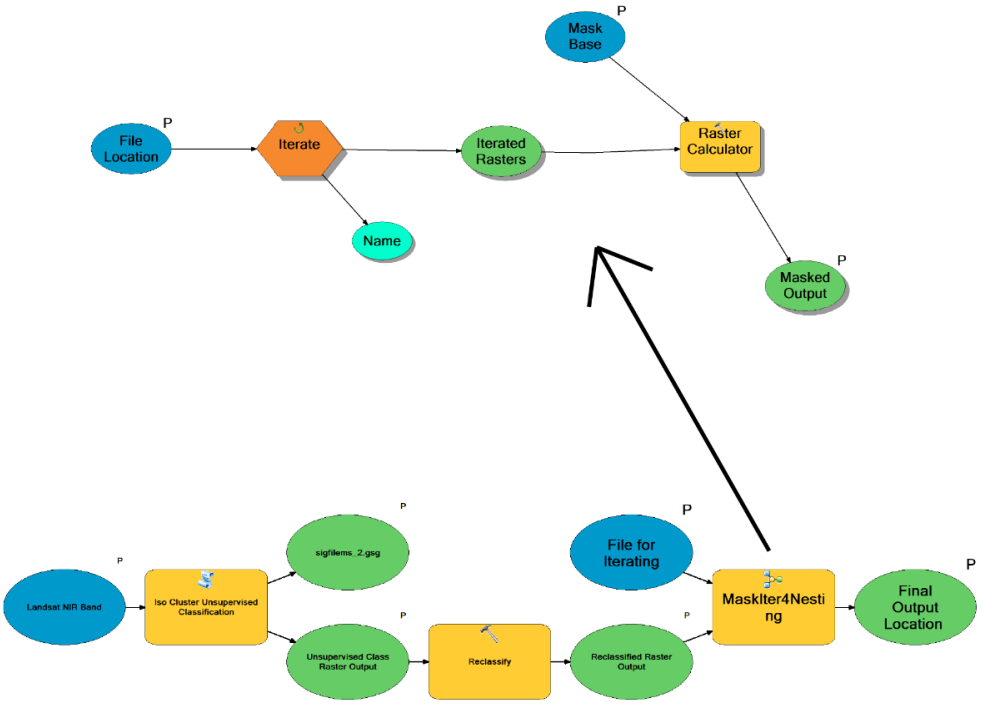

Figure 8: Land masking model

that contains an iterator, that generated a list of raster files for a file location, and a raster calculator function. The raster calculator function was used to multiply the reclassified raster against the iterated raster files, thus generating a water feature only raster data set.

6 *Landsat Surface Water Temperature*

Selected Landsat scenes from 2016, 2018, and 2019 were processed to calculate surface water temperature. This calculation took place inside of a model generated in ArcMap ModelBuilder. Depending on which Landsat collection and scene being processed, one of three models: Landsat 4-5TM (Figure 9), Landsat 7 (Figure 10), and Landsat 8 (Figure 11) were used

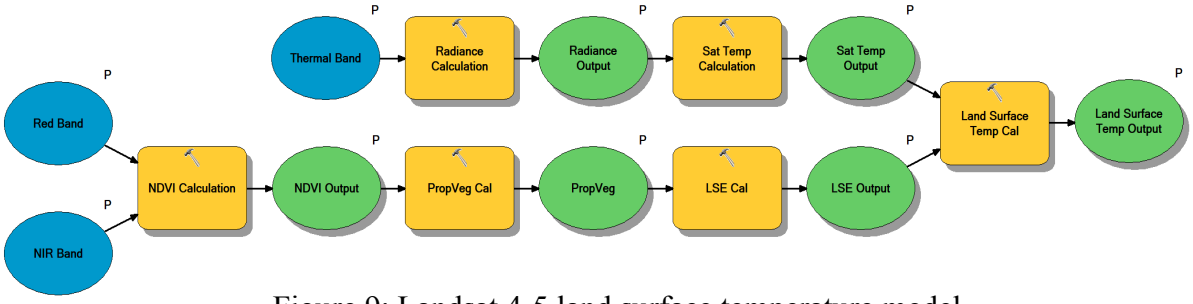

Figure 9: Landsat 4-5 land surface temperature model

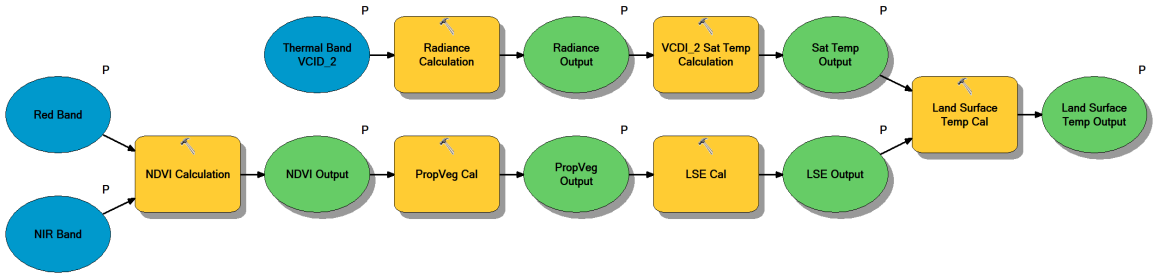

Figure 10: Landsat 7 land surface temperature model

to calculate surface water temperature. The surface water temperature model consists of six

calculations: Normalized Difference Vegetation Index (NDVI), Top of Atmosphere (TOA) radiance, at satellite brightness temperature, proportional vegetation, land surface emissivity, and

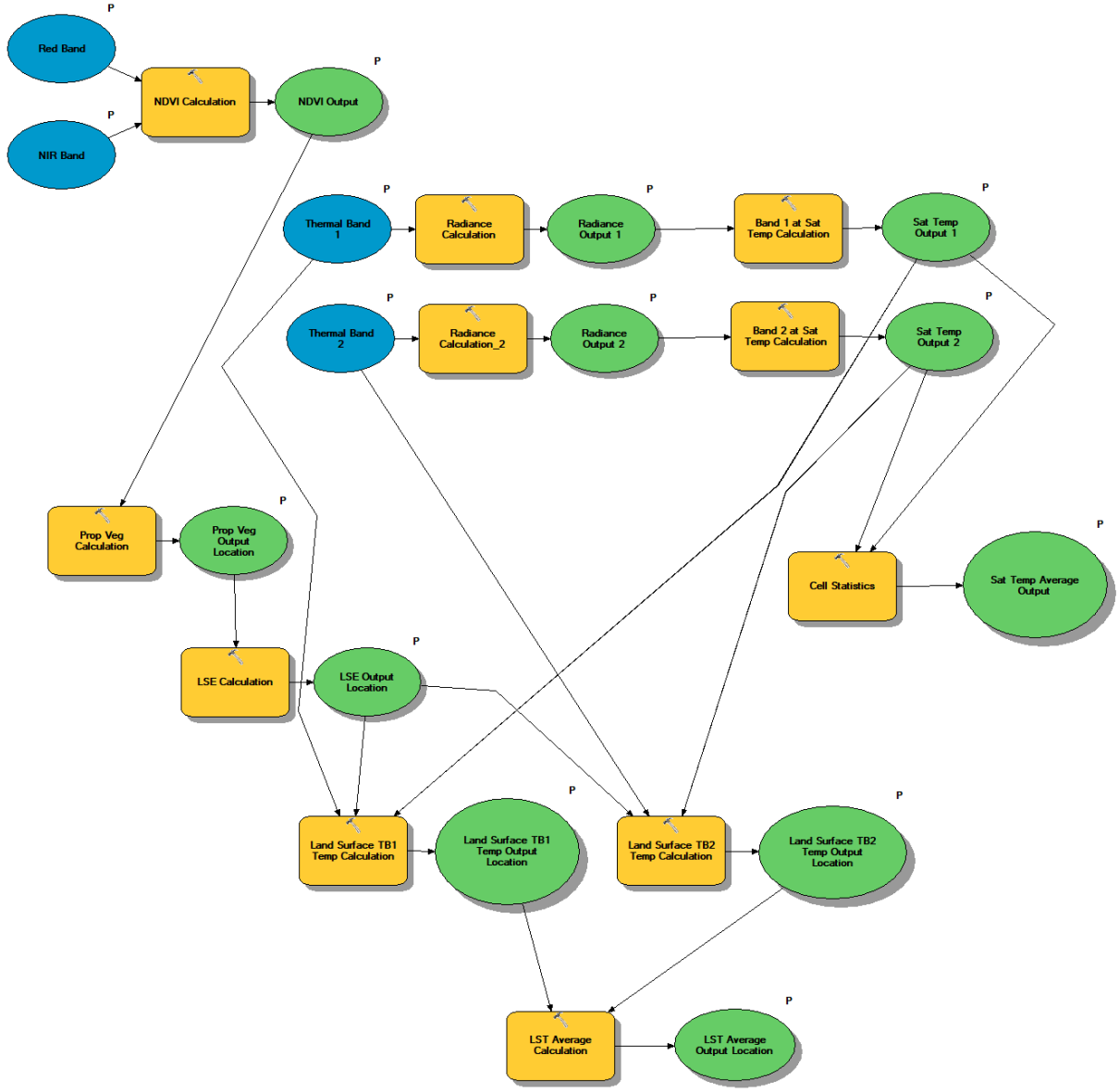

Figure 11: Landsat 8 land surface temperature model

land surface temperature. The first calculation of NDVI is completed by taking the input parameters of a selected Red band and near infrared (NIR) band using the following equation:

$$NDVI = \frac{(NIR-Red)}{(NIR+Red)}.$$

TOA radiance was calculated by using the input parameter of a selected thermal band and the following equation:

$$L_\lambda = M_L Q_{cal} + A_L, \text{ where:}$$

L_λ represents the TOA spectral radiance,

M_L and A_L both represent the band-specific multiplicative/additive rescaling factor from the selected scene metadata.

Q_{cal} represents quantified and calibrated standard product pixel values (Digital Numbers (DN)), from the input parameter of a selected thermal band.

At sensor brightness temperature was calculated next by taking the output parameter of the TOA Radiance calculation and applying it to the following equation:

$$T = \frac{K_2}{\ln\left(\frac{K_1}{L_\lambda}+1\right)} - 272.15, \text{ where:}$$

T represents the at-satellite brightness temperature (K).

L_λ represents the TOA spectral radiance,

K_1 and K_2 represent the band-specific thermal conversion constants from the selected scene metadata, and 272.15 Kelvin is subtracted from the whole equation to convert from Kelvin to Celsius.

Proportional vegetation is calculated using the equation:

$$P_V = \left(NDVI - \frac{NDVImin}{NDVImax} - NDVImin\right)^2, \text{ where:}$$

$NDVI_{min}$ and $NDVI_{max}$ values are obtained from the previously processed NDVI.

Land surface emissivity is calculated with the following equation:

$$e = 0.004Pv + 0.986, \text{ where:}$$

Pv is the proportion of vegetation. Finally, land surface temperature can be calculated by using the following equation:

$$LST = \frac{BT}{(1+W)*\left(\frac{BT}{p}\right)*\ln(e)} \text{ . Where:}$$

BT is the at satellite temperature output,

W is the wavelength of emitted radiance of selected thermal band,

e is land surface emissivity

$$p = h * \frac{c}{\sigma},$$

h is Plank's constant (6.626×10^{-34} J*s)

c is the velocity of light (3×10^{8} m/s), and

σ is the Boltzman constant (1.38×10^{-23} J/K).

The major difference between the three models are the constants of K_1 and K_2 and M_L and A_L which are band-specific thermal conversion and band-specific multiplicative/additive rescaling factors. These constants are populated relative to which Landsat collection is processed through each respective model, however they are not updated with each Landsat scene metadata. These constants are not updated, with each respective Landsat scene, due to insignificant differences in the constant value between scenes. The last major difference is with the Landsat 8 model, where

there are two thermal bands present in the Landsat data. Due to the presence of two thermal bands, TOA radiance, at-sensor brightness temperature, and land surface temperature calculations are repeated. The at-sensor brightness temperature and land surface temperature are then averaged to get one at satellite brightness temperature and land surface temperature. This is completed by using Cell Statistics inside ArcMap which takes the two outputs for average at satellite temperature and land surface temperature and calculates the mean of the respective inputs.

7 Post Model & Single Band/Multispectral Scene Processing

Post model processing involved importing the land surface temperature raster model outputs into ERDAS IMAGINE 2016. In ERDAS IMAGINE the raster land surface temperature of both Mississippi and Louisiana scenes were mosaicked to create one image for analysis using a seamless mosaic in MosaicPro. This single image was then classified into 7 classes in ArcMap.

Single band spectral data processing was needed to extract band 1 spectral values to perform single band spectral analysis across transects of the plume from Bonnet Carre Spillway. This involved extracting two Sentinel 2 Band 1 scenes into ERDAS and completing the same seamless mosaic. Once the images were mosaicked, the image was imported into ArcMap where image transects were created. Once the transects were created, the data were extracted and imported into Excel.

Multispectral data processing was needed to extract band values to perform multispectral visual analysis on Landsat data and multispectral analysis on Sentinel 2 data. Both the Landsat data and Sentinel 2 data were first stacked in ERDAS IMAGINE using the Layer Selection and Stacking tool. The bands that were stacked for the Landsat and Sentinel 2 data to create a multispectral image were bands: 1 - 9, and bands: 1- 10 respectively. The multispectral images

were then processed in ENVI using the Spectral Profile tool was used to select points and generate spectral profiles for Bands 1 – 10 of Sentinel 2 data. Lastly, visual analysis of the multispectral data was completed by opening the stacked Landsat data in ArcMap and selecting the band combination of: Red = Band 3 – Green, Green = Band 4 – Red, and Blue = Band 5 – Near Infrared (NIR), to visually track water influx into the Mississippi Sound.

IV RESULTS & DISCUSSION

1 2018 Bonnet Carre Study Data

Three graphs were generated from the 2018 Bonnet Carre Spillway data collection event. Figure 12 shows Specific conductance (SC) in Microsiemens per Centimeter (µS/cm), Figure 13

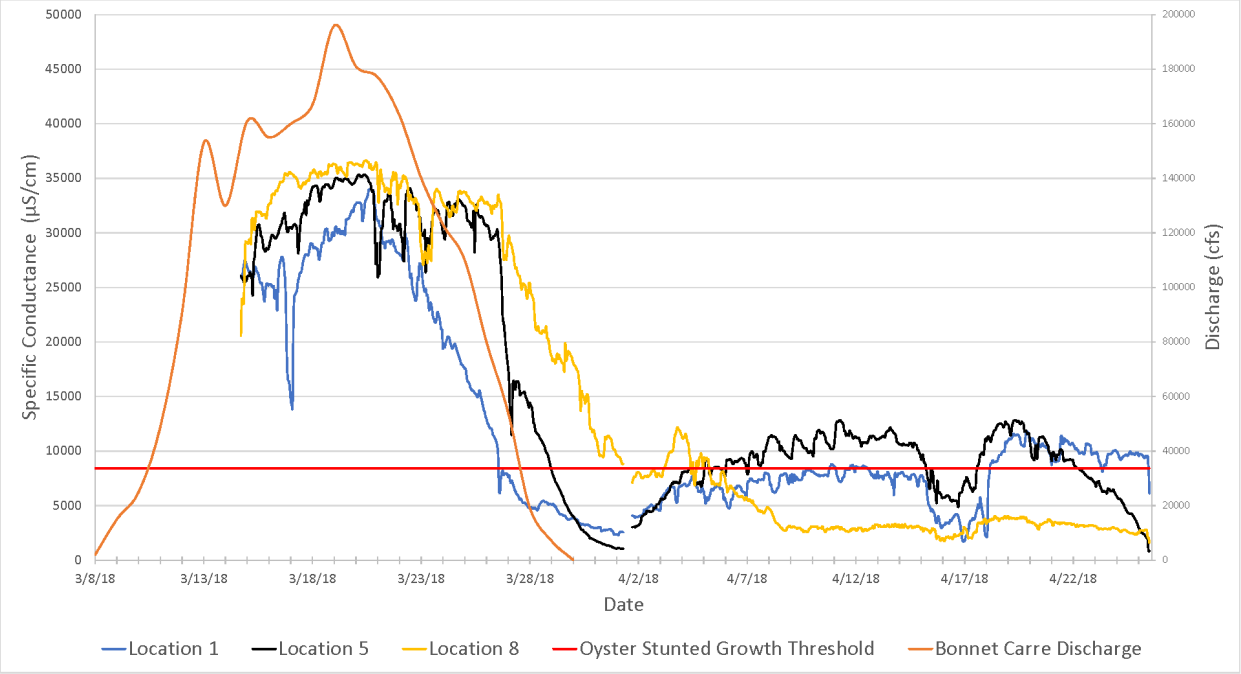

Figure 12: Specific conductance (µS/cm) for the 2018 Bonnet Carre collection event

shows dissolved oxygen (DO) in milligrams per liter (mg/L), and Figure 14 shows temperature in degrees Celsius (°C) for three locations 1, 5, and 8. A location subset was used to display similarities or differences in data relative to distance from the Mississippi shoreline. In addition to a location subset an hourly subset was used to smooth the data curves and the Bonnet Carre

Spillway discharge was added on a secondary axis to give context to opening/closing date and peak discharge dates.

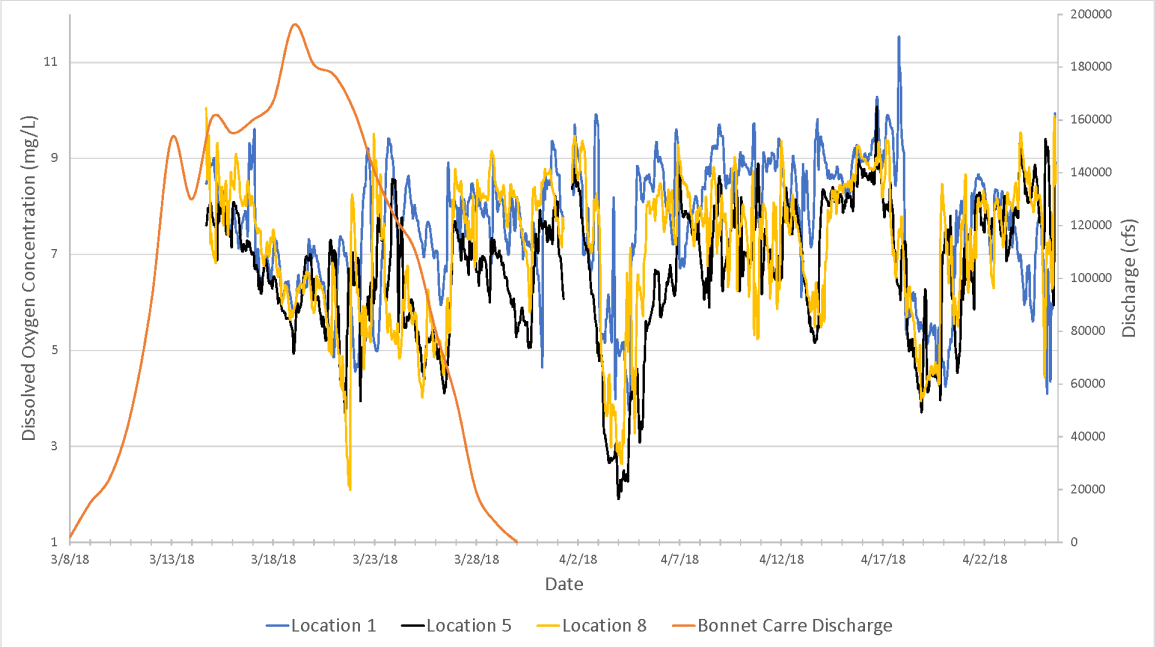

Figure 13: Dissolved oxygen (mg/L) for the 2018 Bonnet Carre collection event

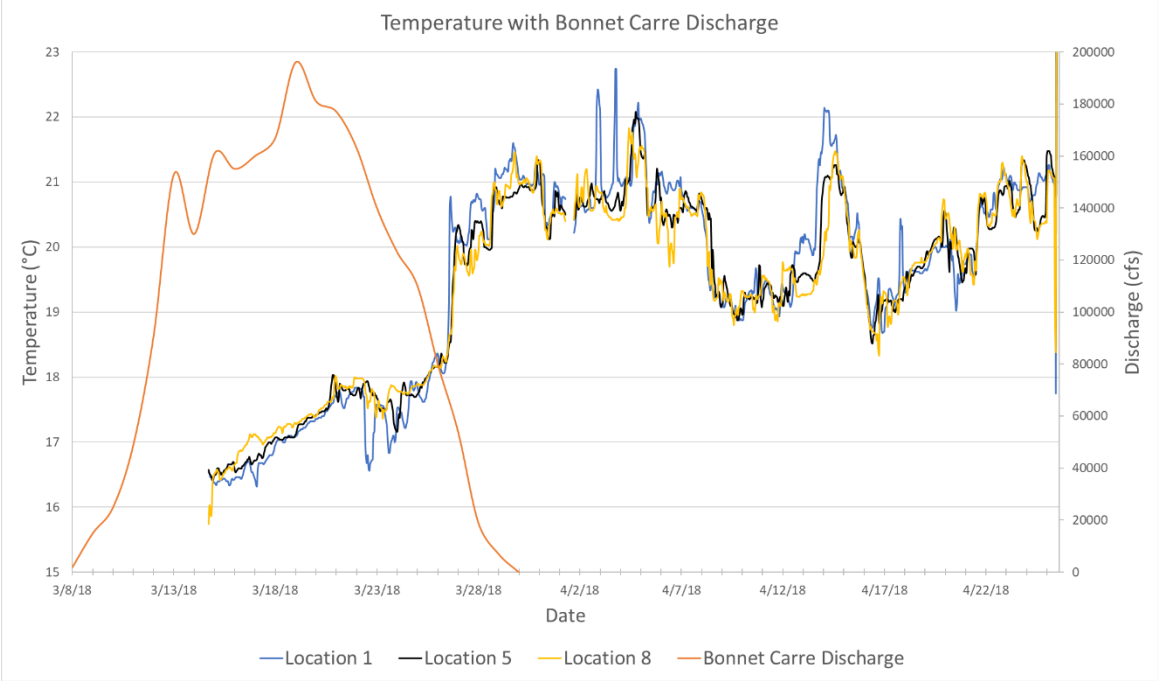

Figure 14: Temperature (°F) for the 2018 Bonnet Carre collection event

SC is proxy for salinity (ppt) as the conductivity of a water sample is proportional to its ion concentration thus salinity, and is an easier parameter to record. Also, SC was used instead of

salinity due to the ability to perform a comparison to USGS SC sensor in our study area. The SC data showed a significant decrease in SC starting on 3/21/18 at location 1, followed by another significant decrease in SC at locations 5 and 8 on 3/27/18. SC displays an increase beginning on 4/1/18 at locations 1 and 5. SC at location 8 has a small increase on 4/3/18, but immediately decreases again on 4/4/18 and remains low for the remaining data collection period. At locations 1 and 5 a significant decrease in SC is recorded from 4/14/18 until 4/18/18. After 4/18/18 the SC levels is stable for location 1, but the levels at location 5 decreases starting 4/21/18 until the end of the data collection.

The significant decrease observed for location 1 on 3/21/18 and locations 5 and 8 on 3/27/18 is believed to be the water influx from the Bonnet Carre Spillway. The delay in initial decrease at locations 5 and 8 are not currently understood, however from multispectral analysis completed below it has been observed that the Bonnet Carre Spillway plume stayed near the coastline before advancing into the surrounding area (Figure 27). This interpretation is also supported by multispectral analysis completed on a Sentinel 2 image from March 19, 2019 (Figure 15). This image, which is being used as a proxy for the 2018 Bonnet Carre Spillway opening, shows that the plume reaches beyond our 2018 study area within 20 days, thus our interpretation of a first influence in our data on 3/21/18 is valid. An increase in SC at locations 1 and 5 on 4/1/18 is also not fully understood, but could be the result of stronger nearshore currents causing a temporary recovery from the freshwater influx of the Bonnet Carre Spillway. This slight recovery is not observed by location 8. The significant decrease observed at locations 1 and 5 from 4/14/18 until 4/18/18 is the result of a significant rainfall event lowering the salinity of the water (Appendix A Figure 35a).

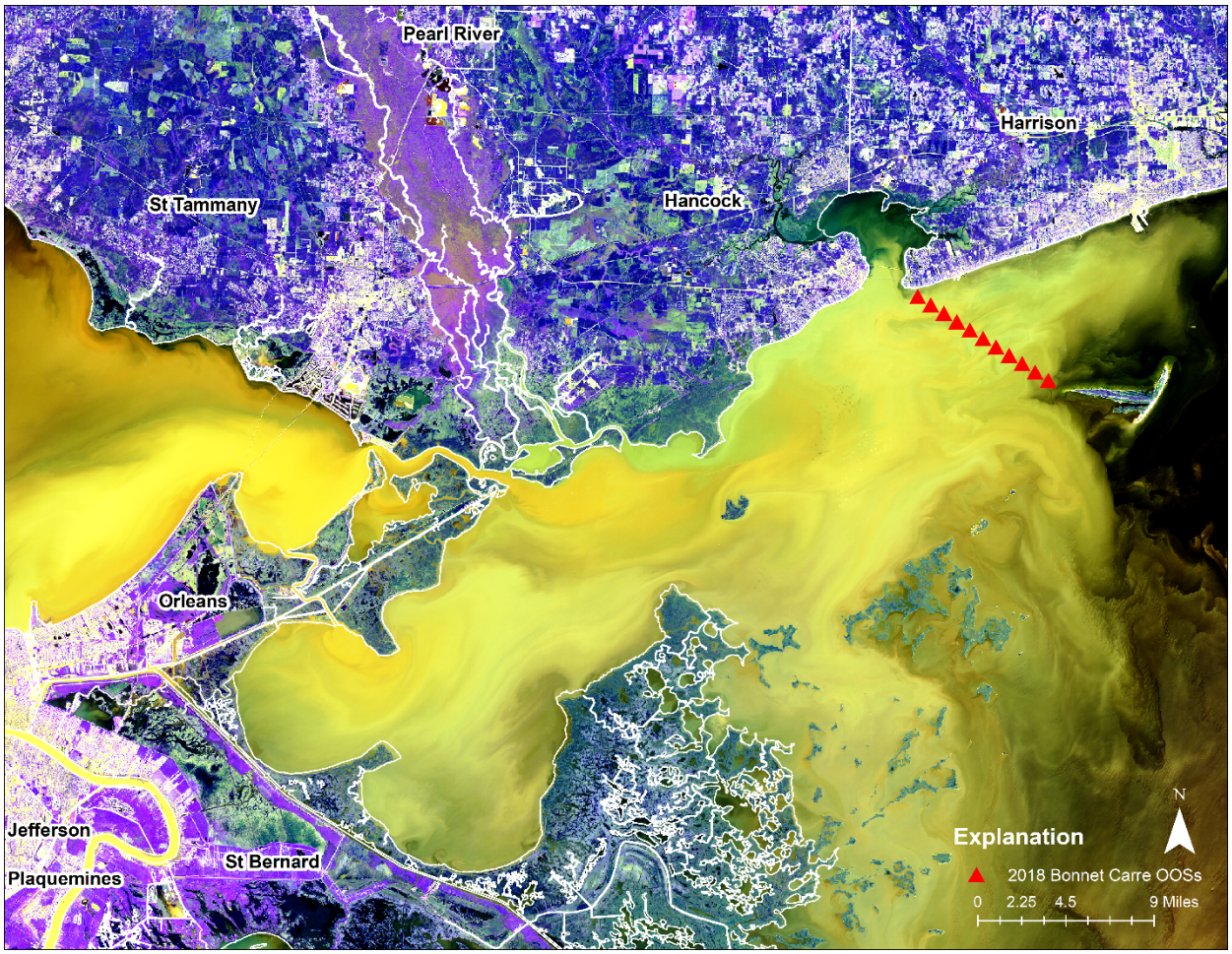

Figure 15: 2019 Sentinel 2 plume extent proxy image for 2018 Bonnet Carre Spillway opening

The DO sensors recorded significant decreases on 3/21/18 only at location 8, while location 1 and 5 remain consistent. A secondary decrease can be observed for all locations starting 4/1/18 with an initial increase starting 4/4/18. A third decrease for all locations can be observed starting 4/17/18 with increase occurring on 4/19/18.

The significant decreases observed are difficult to relate to the Bonnet Carre Spillway plume, primarily due to data noise. As a result of this we have determined that DO is not significantly impacted from the opening of the Bonnet Carre Spillway. This interpretation is supported by the lack of a similar response timing as SC and temperature with the opening of the Bonnet Carre Spillway. The only confirmable decrease observed at all locations was the event

starting on 4/17/18 and ending on 4/19/18 which is interpreted as a short-term water column stratification caused by a significant rainfall event (Appendix A Figure 36a).

Temperature is recorded to increase at all locations during the start of data collection with a significant increase observed occurring between 3/26/18 and 4/8/18. A secondary significant increase in data is seen between 4/13/18 and 4/15/18 followed by a significant decrease starting on 4/15/18 until 4/17/18. After 4/17/18 temperature is observed to stabilize with minor variation.

The significant increase at all locations during the start of data collection followed by stabilization is due to the natural temperature increase of the Mississippi Sound when transitioning from spring to summer. This is confirmed by USGS buoy data which displays a similar trend. The significant increase observed at all locations for the time period of 3/26/18 until 4/8/18 is the result of Bonnet Carre Spillway plume, due to the significant deviation from normal temperature fluctuations and trend, thermal analysis discussed below, and 2019 Sentinel 2 proxy image discussed above (Figure 15). The Sentinel 2 proxy image validates the timing of first influence. The second significant increase in temperature is currently not fully understood. Lastly, a secondary decrease starting on 4/15/18 until 4/17/18 is the result of a significant rainfall event, which would likely lower water temperature (Appendix A Figure 37a).

2 Data Validation

The in-situ data for SC and temperature for 2018 Bonnet Carre Spillway study were compared to USGS station data of the same values and study period, to validate data observations. In addition to an observational comparison, the data for both sites were also

compared using a Pearson statistical test in Excel. A Pearson statistical test is a test to understand how well two datasets are correlated. The USGS station used for comparison was the Merrill Shell Station which is located approximately 2.2 miles south-west from our study sites (Figure 16) and has the USGS station code of 301429089145600. The USGS station sensor types and sampling method are unknown for this comparison, however comparison of DO was not possible due to a lack of the sensor on the USGS buoy.

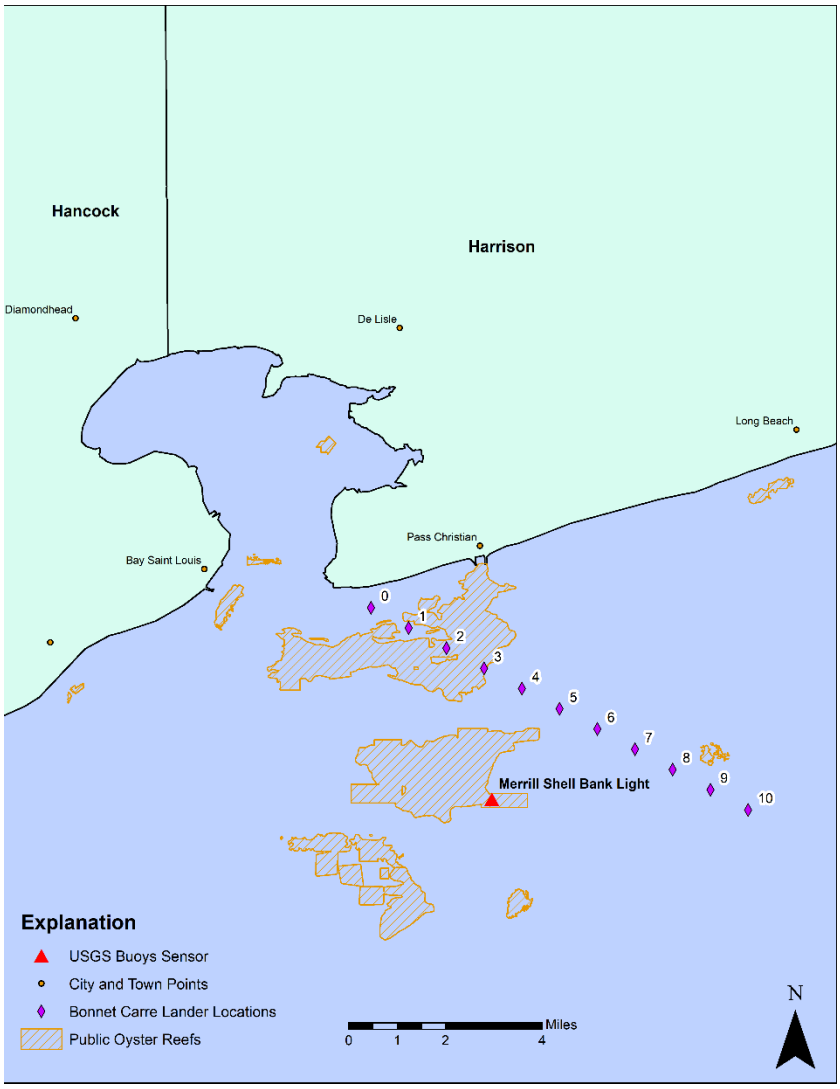

Figure 16: USGS Merrill Shell sensor station

Figure 17 shows the comparison of SC between the 2018 Bonnet Carre study sites 1, 5, and 8 and the USGS Merrill Shell station. The USGS Merrill Shell station had a lower SC measurement at the start of the 2018 Bonnet Carre study. The remainder of the data is comparable. The USGS data is highly correlated to location 1 data, while at the same time being the inverse relationship for location 5 over the period of 4/3/18 – 4/11/18. The USGS data is

poorly correlated with data from location 8. After 4/18/18 the USGS data deviate substantially from the data collected in this project, with SC increasing. The Pearson correlation value for the time period of 3/14/18 – 4/25/18 is 0.304, which indicates that the USGS and 2018 Bonnet Carre

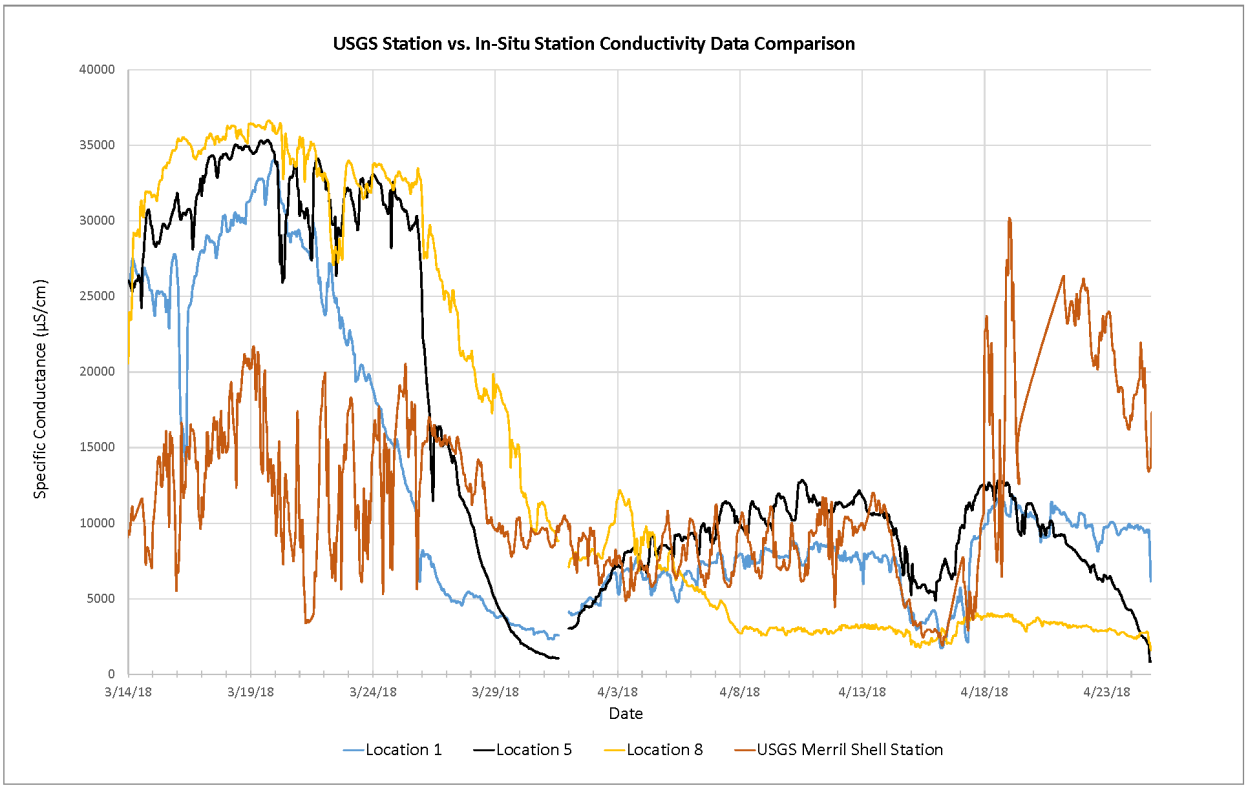

Figure 17: Specific Conductance (µS/cm) comparison between USGS Merrill Shell station data and 2018 Bonnet Carre Study data

Spillway data have a positive correlation, however there is a significant discrepancy between the datasets. If a limited Pearson test is completed on the two datasets, which excludes data after 4/18/18, the correlation value increase to 0.635.

The starting lower measurements of the USGS sensor is not fully understood, but could be the result of two different sampling methods. The USGS sensor samples the water at 25 degrees Celsius which may result in a more accurate measurement when compared to our measurements which is under the influence of the variable temperatures of the Mississippi Sound. The USGS data after 3/31/18 and until 4/18/18 is observed to be highly correlated to

location 1 measurements, while for locations 5 an inverse relationship is observed and not fully understood. The lack of a relationship at location 8 to the USGS data is also not fully understood, but maybe due to the location of the USGS sensor which is located roughly 2.2 miles away. The Pearson correlation value for the time period of 3/14/18 – 4/25/18 is not an accurate representation of correlation due to it including data from the USGS which is significantly different from our recorded data set. However, whenever a limited Pearson correlation test is applied, which excludes USGS data after 4/18/18 the correlation value increases to 0.635. This data was excluded as it appears to be a significant sensor malfunction. The correlation value is significant as the closer the value is to 1 the higher the correlation between the two datasets. Figure 18 shows the comparison of Temperature (°C) between the 2018 Bonnet Carre study sites 1,5, and 8 and the USGS Merrill Shell station. The temperature for the USGS Merrill Shell station is observed to have a slightly lower starting measurements than the 2018 Bonnet Carre study, with the main similarities in data occurring after 3/20/18. After 3/20/18 little variation is seen between locations 1,5, and 8 and the USGS Merrill Shell station. The Pearson correlation value for the time period of 3/14/18 –

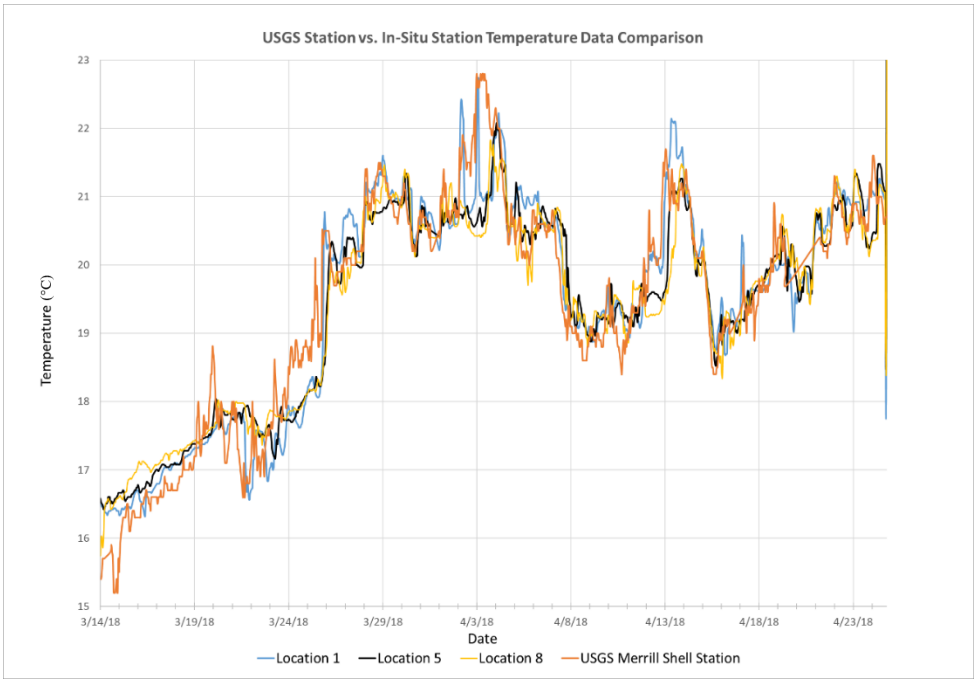

Figure 18: Temperature (°C) comparison between USGS Merrill Shell station data and 2018 Bonnet Carre Study data

4/25/18 is 0.890, which indicates that the USGS and 2018 Bonnet Carre Spillway Data has a significant correlation.

The observed lower starting temperature of the USGS station could be attributed to minor sensor differences, but is not significant. The Pearson correlation value of 0.890, is highly significant and indicates that the two datasets are highly correlated and is attributed to similar spatial extent and sampling methods.

3 Sentinel 2 Multispectral and Single Band Data

Sentinel 2 imagery from the 2016 (Table 3) Bonnet Carre Spillway opening events were used to generate multispectral curves for eight sites: The Mississippi River, Bonnet Carre plume, center of Lake Pontchartrain, West Rigolets, East Rigolets, the Pearl River, Bay St. Louis, and the Bonnet Carre Spillway 2018 Study Sites (Figure 19), to see how freshwater influx effects multispectral responses. These locations were chosen based on observations of multispectral imagery of the Bonnet Carre Spillway plume characteristics during current and historic openings to ensure full sampling of the Bonnet Carre Spillway plume.

Figure 19: Multispectral imagery sampling locations

Table 3: Sentinel 2 multispectral and single band analysis imagery collection dates

	Open	Closed

Mississippi	01/17/16 03/14/18	01/04/16 03/04/18
Louisiana	01/17/16 03/12/18	01/04/16 03/07/18

Figure 20 shows the multispectral response for 2016 when the Bonnet Carre Spillway was closed (solid lines) and opened (dashed lines). It can be observed that when the plume

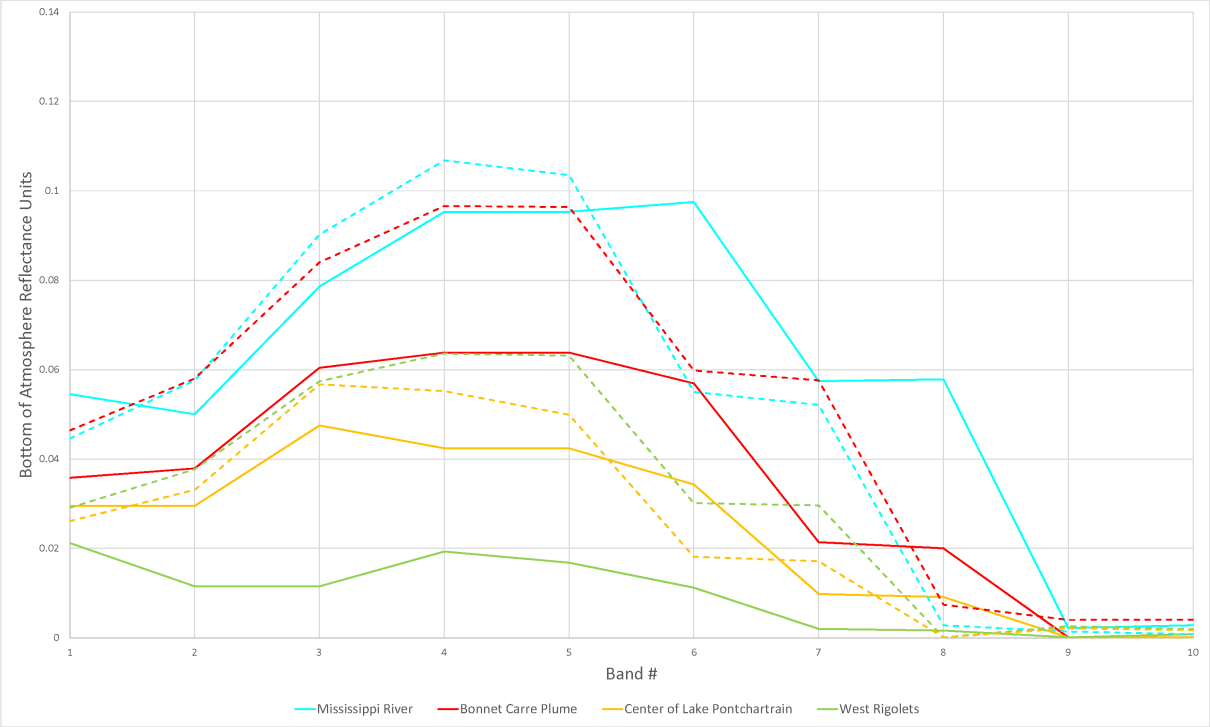

Figure 20: Multispectral Response Curves for the 2016 closed and opened Bonnet Carre Spillway

mixes with Lake Pontchartrain water, there is a significant increase in spectral response in bands 3 (Green), 4 (Red), and 5 (NIR) due to the increase in sediment and suspended material in the water. The water in other sampled locations does not show as high of response due to sediment in the water. The spectral response for all locations approaches zero in band 8 except for the Bonnet Carre Spillway Plume and Mississippi River spectral response, which is seen to have a significant decrease following band 8 to zero at band 9, indicating higher sediment content in the water. Lastly, as the water from the spillway continues to move across Lake Pontchartrain, the

impact of the increased sediment load and the resulting increase in spectral response will decrease as the water from the Mississippi River mixes with the brackish water in Lake Pontchartrain.

An increase in reflectance at each sampling location (excluding the Mississippi River), of the opened spectral response, can be observed, however each sampling location has a different magnitude of reflectance increase. At the time of image acquisition the Bonnet Carre Spillway had only been open 8 days and the plume can be seen covering 17.5 kilometers north east of the spillway mouth, and reaching the sampling point Bonnet Carre Plume (Figure 21). Thus the only confirmable impact of the spillway opening can be seen at the Bonnet Carre Plume sampling point. The significant increase in spectral response is due to the high suspended sediment

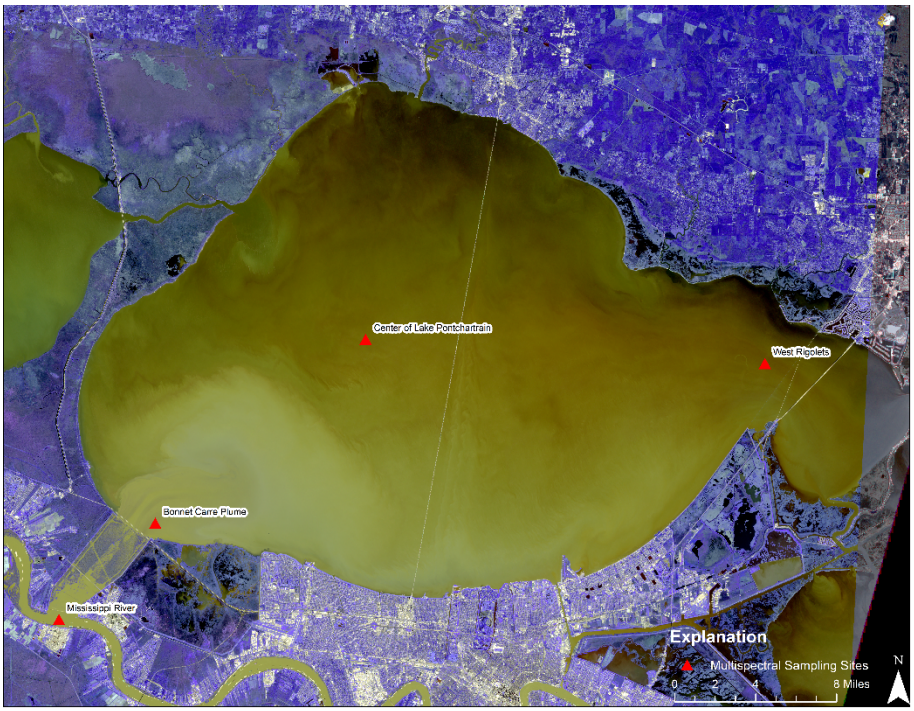

Figure 21: Sentinel 2 image showing Bonnet Carre Spillway plume extent and multispectral sampling locations

concentrations coming from the Bonnet Carre Spillway causing an overall increase in reflectance within the visible and near infrared spectrum. According to Brodie et al,(2010) plume mapping

was possible by analyzing total absorption in the blue spectral region at a wavelength of 443nm for high chlorophyll concentrated water. Thus, if chlorophyll concentrations were high in the Bonnet Carre Spillway plume the reflectance between bands 1 (coastal aerosol) and 2 (blue) would decrease vs. display an increase. The increase observed in the band 3, green spectral range, is due a slight increase in chlorophyll, which absorb blue light and cause green hues in the water. The significant increase in reflectance between bands 4 (red) and 6 (NIR) is the direct result of the Bonnet Carre Spillway plume and/or water mixing, having a high concentration of suspended matter. According to Doxaran et al.,(2003): high concentrations of suspended matter, particularly waters very rich in mineral particles, results in higher reflectance values in the NIR spectrum. The spectral response in bands 6 through 8 do not show significant differences and these bands are therefore not as useful in tracking the Bonnet Carre spillway plume across Lake Pontchartrain and into Mississippi Sound.

A single band 1 spectral response transect was generated for several Sentinel 2 data from the Bonnet Carre Spillway to the Mississippi Sound during the opened and closed Bonnet Carre Spillway events of 2016 and 2018 (Table 3). Figure 22 shows the sampling locations for the Sentinel 2 single band

Figure 22: Single band spectral analysis sampling locations

spectral analysis, to see how freshwater influx effects Sentinel 2 Band 1 response. Band 1 of Sentinel 2 has a central wavelength of 442.7 nm and is equivalent to Ultra Blue (coastal/aerosol).

Figure 23 shows the response curves for Sentinel 2 band 1 for the 2016 and 2018 closed and opened Bonnet Carre Spillway. The band 1 data for 2016 when the Bonnet Carre Spillway was closed shows a progressive decline in reflectance as the transect progresses from Lake Pontchartrain into the GoM, indicating that the water contains less suspended sediment, and thus reflectance is decreasing. The data from the 2016 opening of the Bonnet Carre Spillway open shows a much larger initial spike of reflectance between reference points 0 and 15, roughly the Bonnet Carre Spillway plume, and Lake Pontchartrain, followed by the same progressive decline as the transect progresses into the Rigolets. The data stops at reference point 50 due to a lack of image availability for sampling locations east of the Rigolets. The 2018 Bonnet Carre Spillway

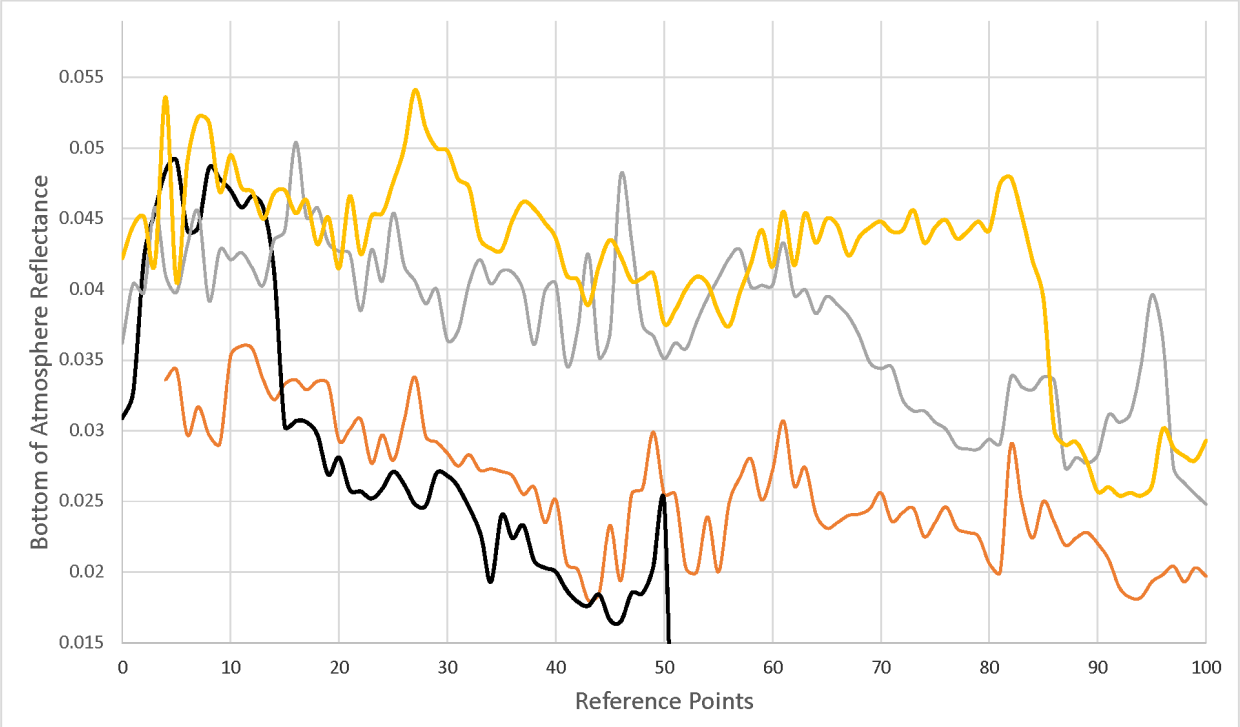

Figure 23: Sentinel 2 Band 1 spectral response curves for the 2016 and 2018 Bonnet Carre Spillway opening events

closed data shows a progressive decline as the transect progresses into the GoM from Lake

Pontchartrain, with only minor peaks occurring at reference point 15 (Bonnet Carre Plume), 45 (East Lake Pontchartrain), and 95 (Gulfport). The 2018 Bonnet Carre Spillway open data shows a less progressive decline into the GoM but rather a very sharp decline after reference point 80 (South of 2018 Bonnet Carre Study), followed by a period of increase.

In summary, whenever the Bonnet Carre Spillway was closed the reflectance decreases as the transect progresses into the Mississippi Sound due to the lack impact from a sediment plume, and lower suspended sediment concentrations. The 2016 open data initial spike in reflectance is the direct result of higher suspended sediment present in Lake Pontchartrain from the Bonnet Carre Plume, however the area with increased reflectance has a limited extent mainly due to the spillway only being open 8 days and was visually confirmed to sampling point 14 (Figure 24). The 2018 opened data displays a peak reflectance due to the Bonnet Carre Spillway opening 4

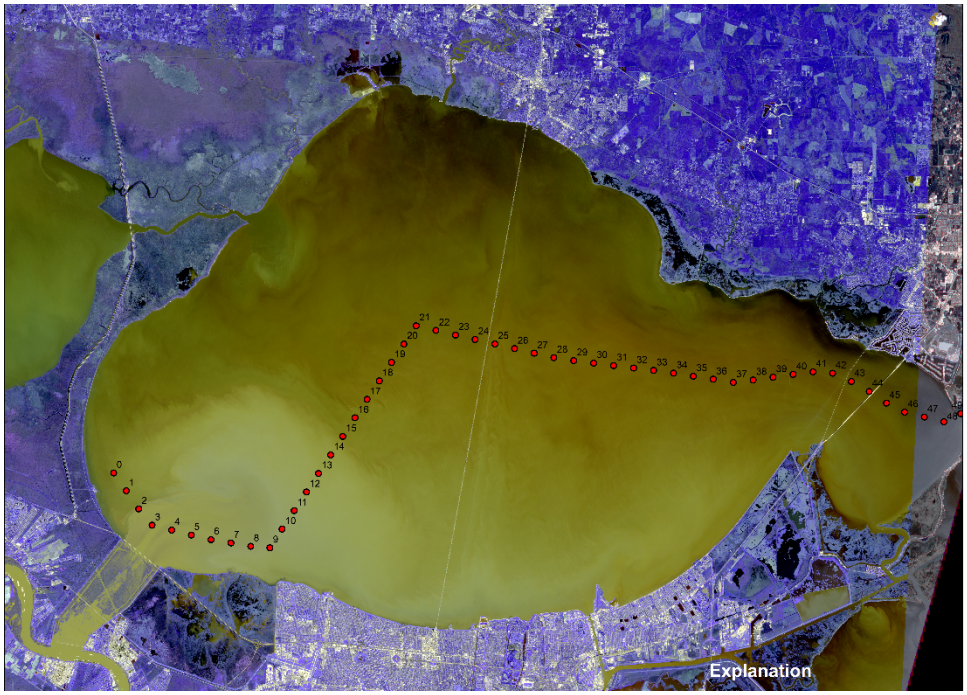

Figure 24: 2016 Sentinel 2 image showing Bonnet Carre Spillway plume extent and Sentinel 2 band 1 sampling locations

days before image acquisition and the Bonnet Carre plume can be seen up to reference point 10

where reflectance can be seen to significantly decrease due to the Bonnet Carre Spillway plume having a limited extent (Figure 25). A secondary spike can be seen between reference point 25 – 30 and is not the direct Bonnet Carre Plume, as the plume is not visibly identifiable, but rather

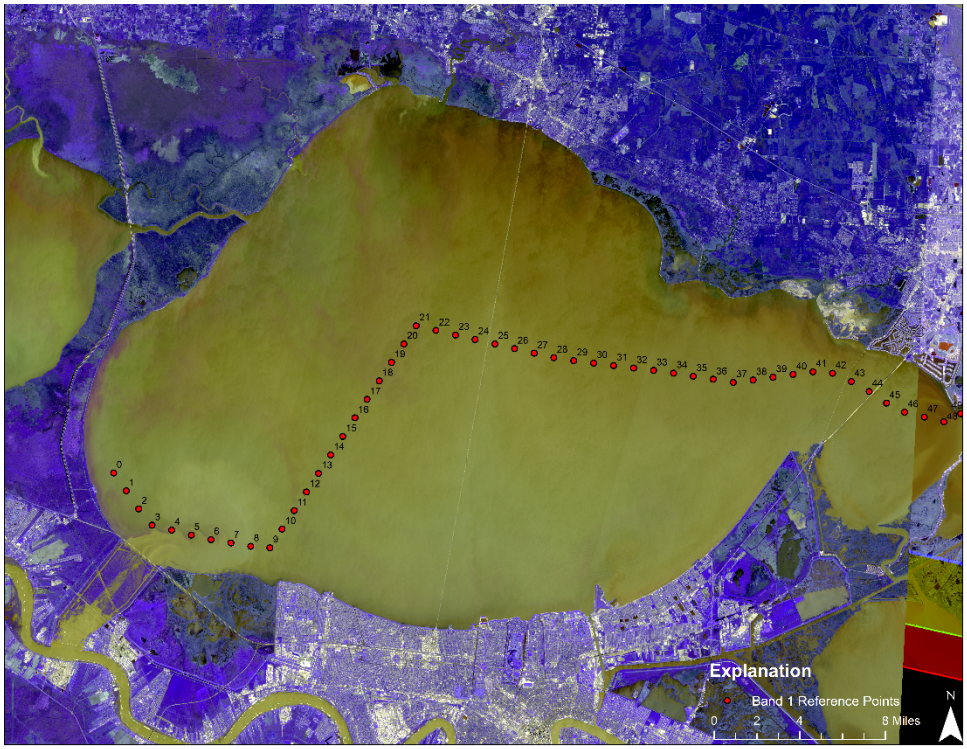

Figure 25: 2018 Sentinel 2 image showing Bonnet Carre Spillway plume extent and Sentinel 2 band 1 sampling locations

the result of the Bonnet Carre Spillway plume and/or resultant mixing and flushing effects on Lake Pontchartrain. Another peak between reference point 80-85 can also be seen, this is from the Pearl River plume and Lake Pontchartrain water mixing into a tertiary plume, rather than directly from the Bonnet Carre Plume due having a limited extent.

4 *Landsat 8 Multispectral Visual Imagery*

Landsat 8 multispectral imagery was analyzed to understand if the Bonnet Carre Spillway and other influxes were visible in Lake Pontchartrain and further into Mississippi Sound. The band combination: Red = Band 3 – Green, Green = Band 4 – Red, and Blue = Band 5 – Near Infrared (NIR) was selected to best display plumes and possible accessory features, such as sediment mixing due to water influx into and out of Lake Pontchartrain. These plumes and accessory feature are visible due to the wavelength of the NIR band for Landsat 8 and the response of water with high concentrations of suspended sediments. Figure 26 is a Landsat 8

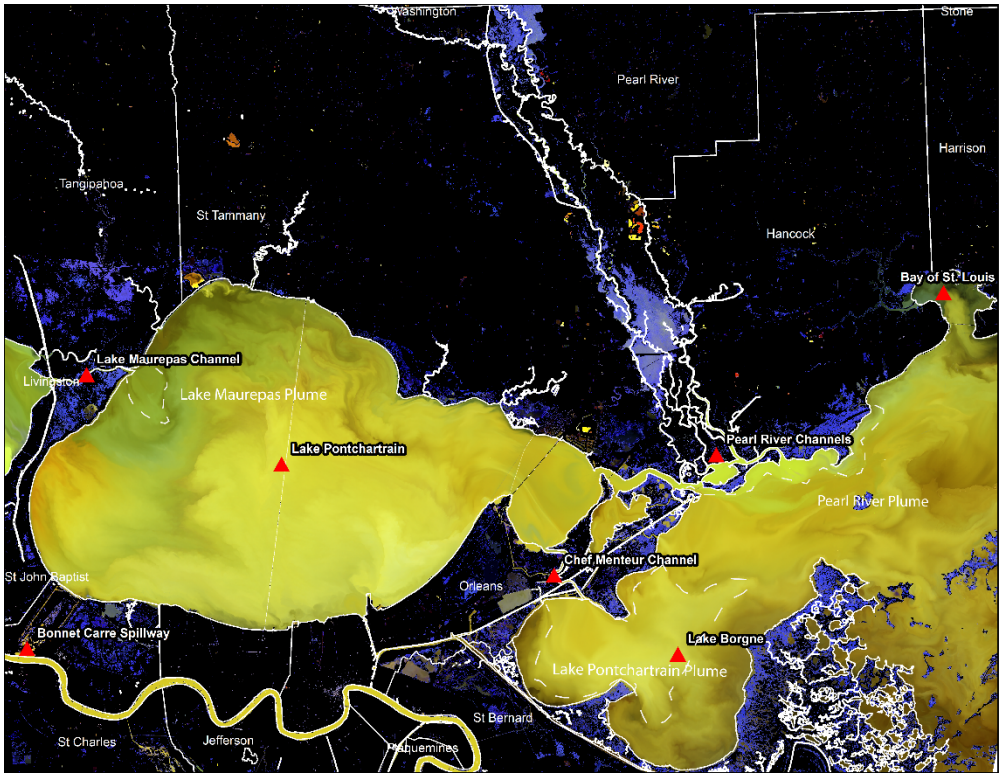

Figure 26: February 10, 2016 Multispectral image with Bonnet Carre Spillway closed

image collected on February 10, 2016, nine days after the Bonnet Carre Spillway closed. The Bonnet Carre Spillway had been open for 22 days and at its peak discharged approximately 203,000 cu ft/s of water into Lake Pontchartrain. Residual water from the Bonnet Carre Spillway channel is entering Lake Pontchartrain, however a plume is hard to distinguish. Influx into Lake

Pontchartrain is visible in the image originating from the Lake Maurepas Channel, which is highlighted by the Lake Maurepas Plume. Lake Pontchartrain displays a mixing of spectral features throughout, with no immediate plume from the spillway. To the southeast influx is visible into Lake Borgne via Chef Menteur Channel originating from Lake Pontchartrain. The Rigolets Channel visible to the north of Lake Borgne has no apparent plume features, however the Pearl River Channels can be seen to have a significant plume migrating into the Mississippi Sound. Figure 27 is a Landsat 7 image collected on January 17, 2016, 7 days after the Bonnet Carre Spillway opened. Water from the Mississippi River is entering the Bonnet Carre Spillway and flowing into Lake Pontchartrain. This Bonnet Carre Spillway plume is highlighted by dashed

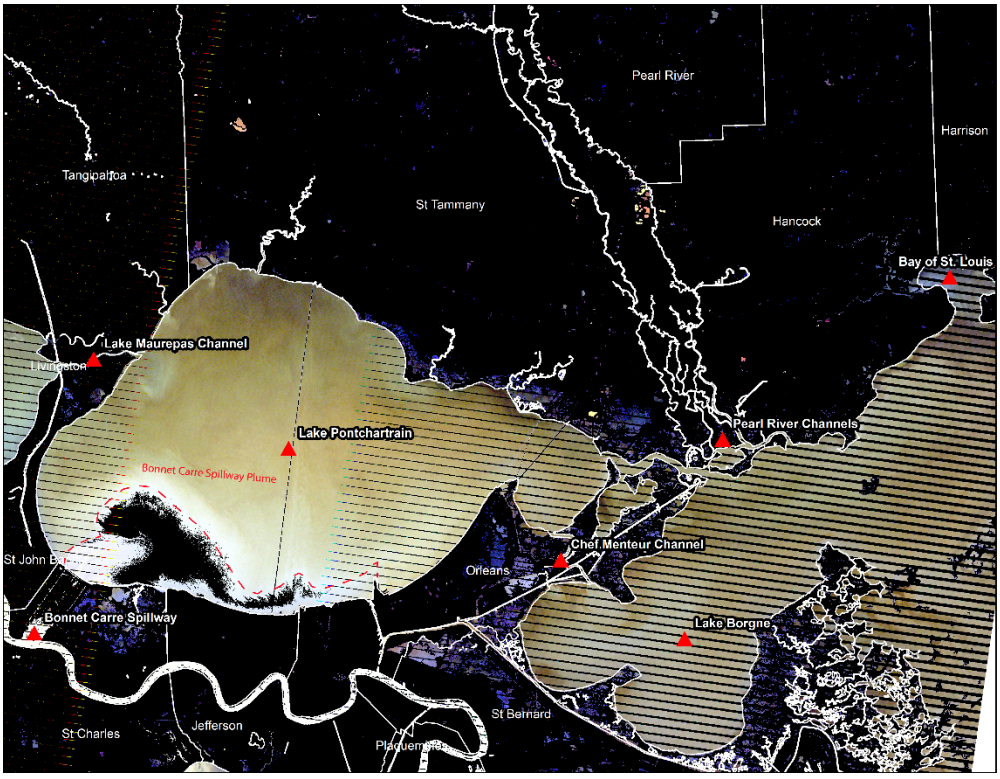

Figure 27: January 17, 2016 Multispectral image with Bonnet Carre Spillway opened

red lines. This is the primary feature of this image, as no other influx is present and the Mississippi River water has not completely mixed.

Figure 28 is a Landsat 8 image collected on March 3, 2018, five days before the Bonnet Carre Spillway was opened. The primary sediment plume is the Pearl River sediment, which shows a plume migrating west into the Rigolets Channel. Secondly, a plume originating from the east most Pearl River channel can be seen extending for a short distance to the south and east. Figure 29 is a Landsat 8 image collected on March 6th, 2019, five days after the Bonnet Carre Spillway opened. Water from the Mississippi River can be seen entering the Bonnet Carre Spillway channel and into Lake Pontchartrain, resulting in the plume highlighted in the image

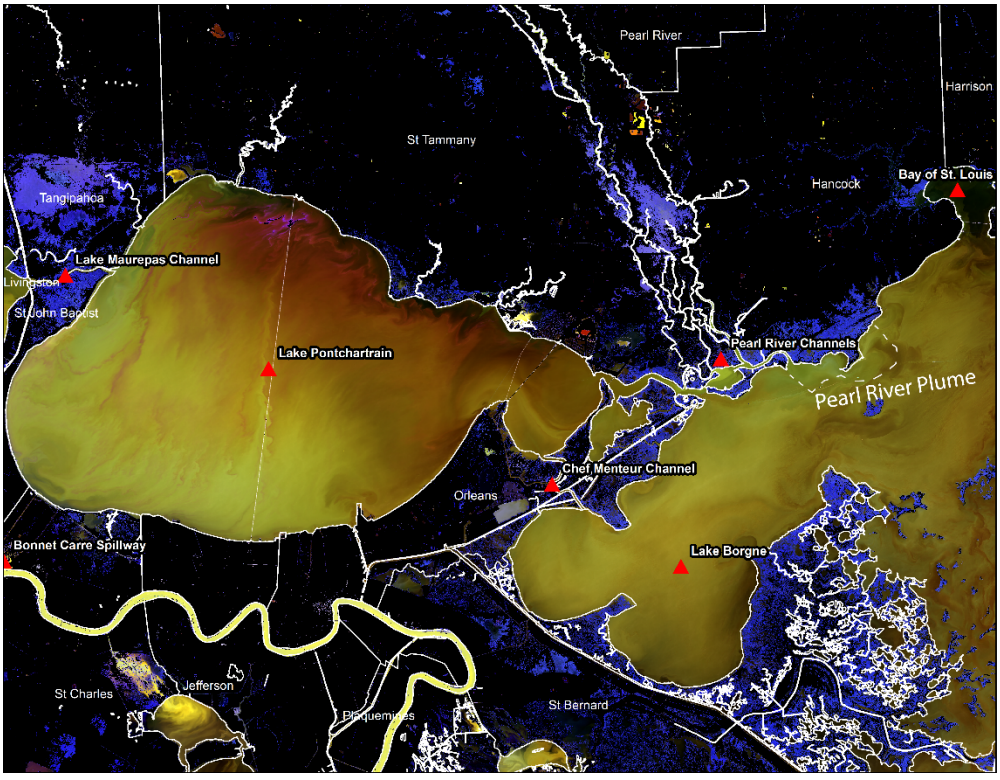

Figure 28: March 3, 2018 Multispectral image with Bonnet Carre Spillway closed

with a white dashed line. No other distinct features can be seen until reaching the Pearl River channels to the northeast. The plume is highlighted by a white dashed line, that nearly reaches

the Bay of St. Louis. The last distinct feature of the image is a plume, of an unknown source, that is visible at the most easterly extent of the image and is not highlighted. Figure 30 is a Landsat 8 image collected on March 22nd 2019, 14 days after the opening of the Bonnet Carre Spillway. Water is still entering the Bonnet Carre Spillway channel and into Lake Pontchartrain causing a

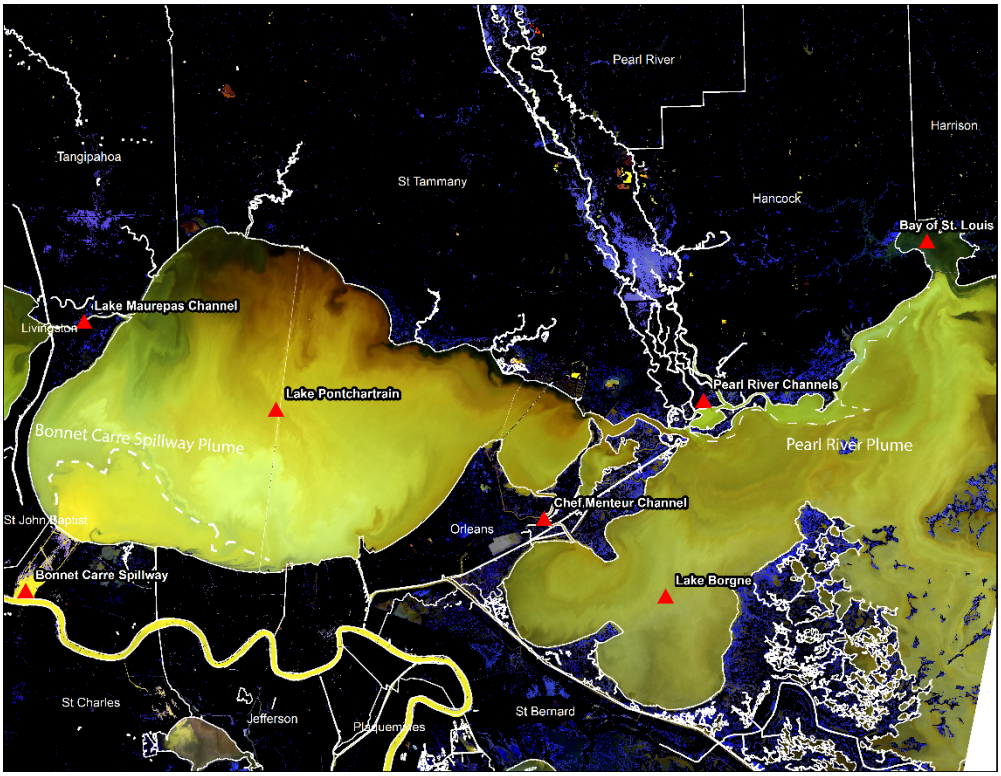

Figure 29: March 6, 2019 Multispectral image with Bonnet Carre Spillway open

plume that distinctly covers approximately half of Lake Pontchartrain and can be seen in the image highlighted by dashed white line. To the northeast the Pearl River channels have a plume migrating east, and again resulting in a plume that nearly reaches the Bay of St. Louis.

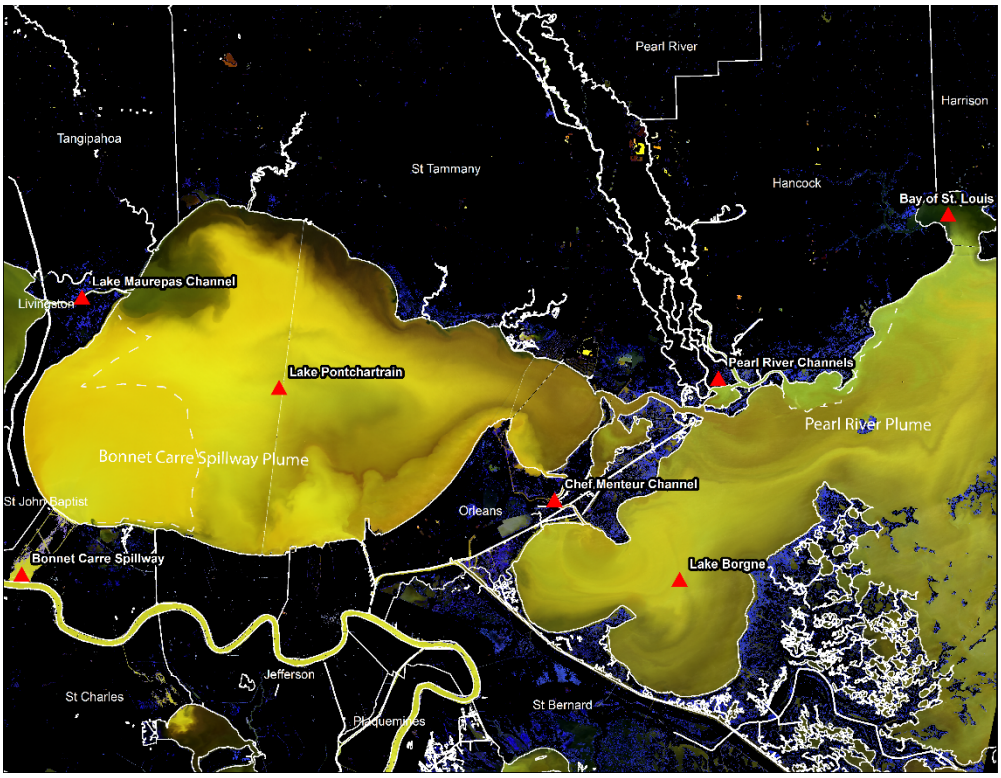

Figure 30: March 22, 2019 Multispectral image with Bonnet Carre Spillway open

To summarize, all plumes visible have an origination from either the Bonnet Carre Spillway, the Pearl River, and/or Lake Maurepas, with the exception of the features visible in the Western Mississippi Sound. These features are a combination of plumes originating from Lake Pontchartrain and the Pearl River, as a direct source is not visible, however it is understood that whenever the Bonnet Carre Spillway is opened Lake Pontchartrain has an increased flushing time. Other features beyond plumes are present in the 2016/2018 Bonnet Carre Spillway closed imagery and not highlighted by dashed lines, as they also have no identifiable source. They are likely the result of either residual water influx and energy and/or normal current occurrences which result in mixing of the water column and sediment suspension. Lastly, an important visible feature present in all of the images is the Pearl River plumes. They can be observed to have moved east whenever the Bonnet Carre Spillway is open and west whenever the Bonnet Carre Spillway is closed. The easterly direction of the plume movement whenever the Bonnet Carre

Spillway is open is due to a large amount of water influx flushing Lake Pontchartrain through the Rigolets Channel and interacting with the Pearl River plume. The westerly direction of the Pearl River plume, whenever the Bonnet Carre Spillway is closed, is due to the normal westerly trending longshore currents pushing the plume into the Rigolets Channel.

5 Thermally Processed Landsat Data

Surface thermal analysis was completed to understand if influxes into the Mississippi Sound were thermally visible. This is completed with a thermal analysis which takes advantage of the thermal bands of Landsat 7 and 8 and the significant temperature difference present between the source water temperature and the receiving water body temperature.

Figure 31 is a Landsat image captured on February 26, 2016, 15 days after the Bonnet Carre Spillway closed. Surface water temperature has a range of 11.64 – 20.0 °C. The average temperature of sampled locations can be seen in Table 5.

Table 4: Thermal analysis sampling locations average temperature (°C)

	February 26, 2016 Temperature (°C)	January 17, 2016 Temperature (°C)	March 3, 2018 Temperature (°C)	March 6, 2019 Temperature (°C)
Bonnet Carre Spillway Plume	X	8.95	X	8.94
Lake Pontchartrain	14.19	11.03	18.96	12.73
Lake Borgne	13.59	11.55	19.21	12.59
Mississippi Sound	14.02	11.35	19.27	12.79

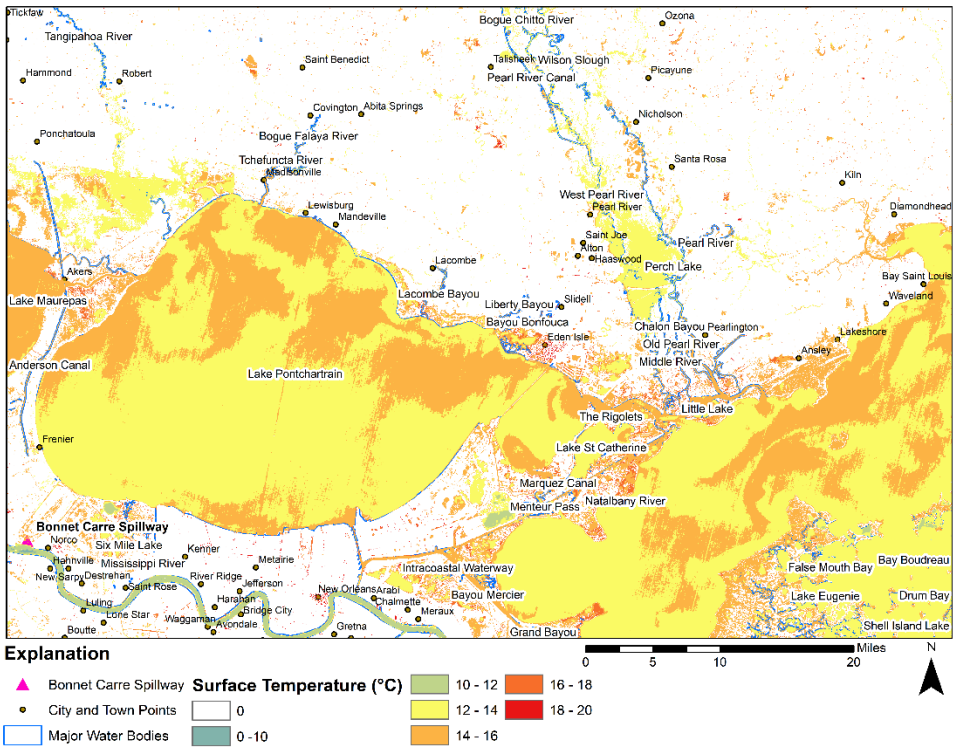

Figure 31: February 26, 2016 Surface water temperature map: Bonnet Carre Spillway closed

Figure 32 is a Landsat 7 image captured on January 17, 2016, seven days after the Bonnet Carre

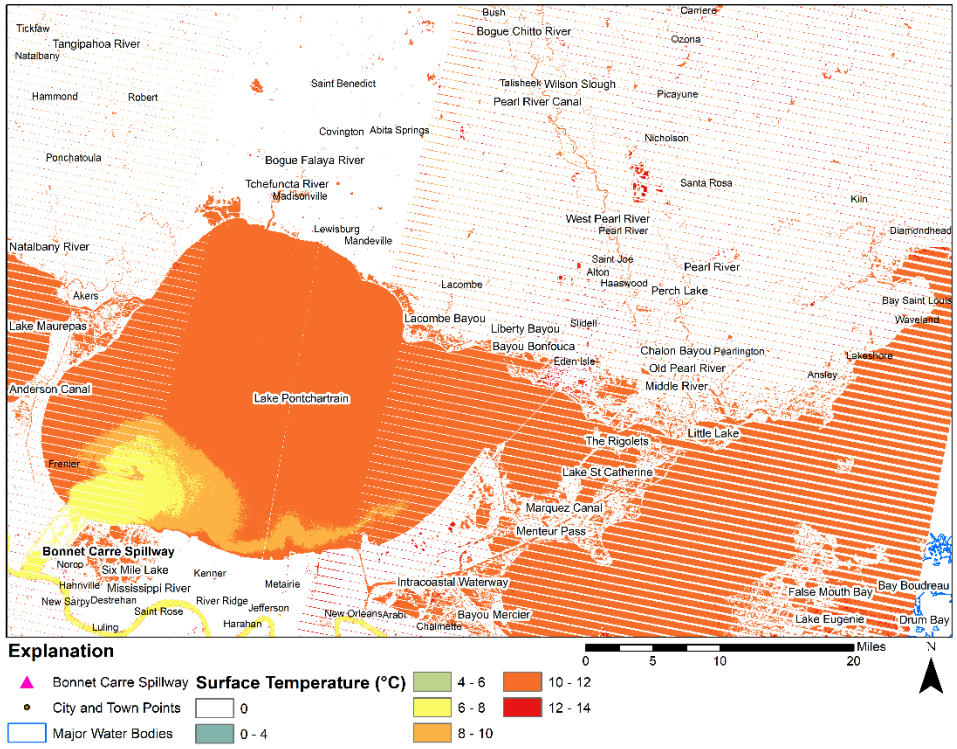

Figure 32: January 17, 2016 Surface water temperature map: Bonnet Carre Spillway opened

Spillway opened. Surface water temperature has a range of 4.22 – 14.0 °C. The average temperatures of sampled locations can be seen in Table 5. The temperature of the water coming from the Mississippi River was approximately 2.08 °C cooler than the water in Lake Pontchartrain resulting in a thermal plume visible in the surface water temperature map for the 2016 Bonnet Carre Spillway opening event. Figure 33 is a Landsat 8 image captured March 3,

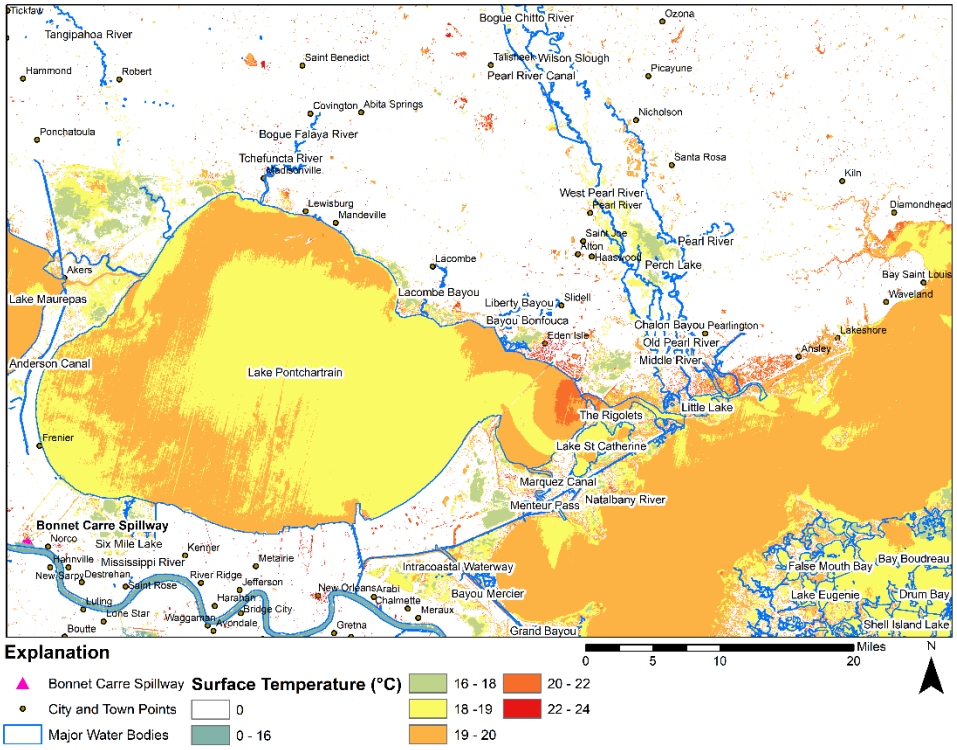

Figure 33: March 3, 2018 Surface water temperature map: Bonnet Carre Spillway closed

2018, five days before the Bonnet Carre Spillway was opened. The surface temperature has a range of 15.84 – 24.0 °C. The average temperatures of sampled locations can be seen in Table 5. The surface water temperature map shows a clear gradient of increasing water temperature as it moves from Lake Pontchartrain into the Mississippi Sound. Figure 34 is a Landsat 8 image capture roughly one year later on March 6th 2019. The surface temperature has a range of 1.28 –

16.0 °C. The average temperatures of sampled locations can be seen in Table 5. The temperature of the water coming from the Mississippi River is approximately 3.80 °C cooler than the water in Lake Pontchartrain. A thermal plume is visible and is the primary feature of the surface water temperature map for the 2019 Bonnet Carre Spillway opening event.

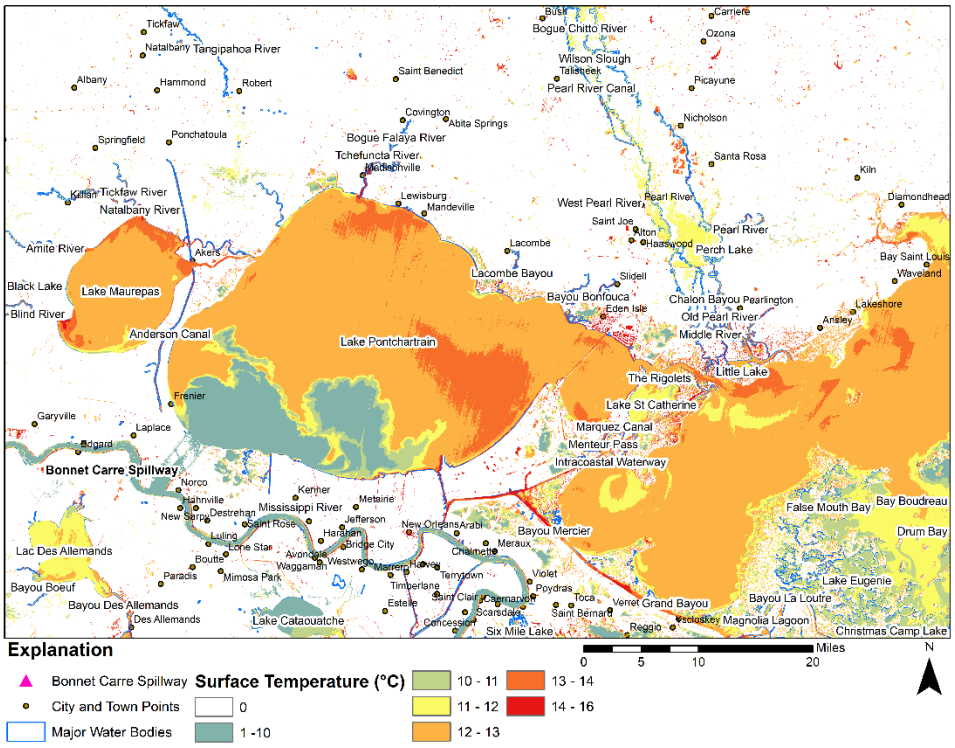

Figure 34: March 6, 2019 Surface water temperature map: Bonnet Carre Spillway opened

In summary, the 2016/2018 closed data results do not show significant water plumes/influxes but rather shows normal surface water temperature. However, for 2018 there is a clear and definite gradient of temperature difference occurring between Lake Pontchartrain and the Mississippi Sound and for 2016 a lack of a temperature gradient. This gradient for 2018 is caused by the temperature difference between the cooler Lake Pontchartrain and the warmer Mississippi Sound. The 2016 closed data lacks to display a temperature gradient due to the image being collected February 26 which still is in winter conditions. For the 2016/2018 opened Bonnet Carre Spillway thermal analysis displays a clear and definite plume originating from the Mississippi

River and into Lake Pontchartrain from the Bonnet Carre Spillway. In addition to the plume a secondary feature is visible in the thermal maps. This feature is the warmer surface temperature surrounding the cooler initial plume. The reason this feature exists is due to the cooler Mississippi River water eventually reaching an equilibrium with the surround warmer water. Lastly, no clear temperature plume features can be seen to be extending from the Bonnet Carre Spillway into the Mississippi Sound, due to image availability.

V CONCLUSIONS

It has been shown that in-situ water quality monitoring stations and sensors in Mississippi Sound can be used to detect the influx of fresh water due to the opening of the Bonnet Carre spillway. Sentinel 2 multispectral analysis of 2019 data provide valid identification of the Bonnet Carre Spillway plume and other plumes in our 2018 study area, but mixing reduces the spectral signature of these plumes as they leave Lake Pontchartrain.

The three remote sensing analyses completed were: Sentinel 2 single band and multispectral analysis, Landsat 8 multispectral analysis, and Landsat thermal analysis. All of which were successful at identifying the Bonnet Carre Spillway plume, however the Landsat 8 multispectral analysis was most successful in detecting the plumes from the Bonnet Carre spillway in Lake Pontchartrain. Identification of the Bonnet Carre Spillway plume, either spectrally or thermally, within the Mississippi sound was not possible, due to higher levels of mixing with Gulf of Mexico water that reduces both the spectral differences and the thermal differences. However, features were present in our study area that were the result of a combination of Pearl River plumes and increased sediment suspension from Lake Pontchartrain flushing out through the Rigolets channel.

Landsat 8 multispectral analysis successfully showed that identification and tracking of plumes are possible for the initial influx, but are later obscured by water column mixing. Landsat thermal analysis successfully showed plume waters originating from the Bonnet Carre Spillway and the Pearl River, due to the significant temperature difference present between the source

water temperature and the adjacent water bodies' temperature, which it flows into. Lastly, this analysis can be used to go beyond multispectral analysis and provide information on plume extent beyond initial influx. Lastly, due to image availability only a 2019 Sentinel 2 proxy image was able to confirm our interpretations of plume timing with in-situ water quality data, however future work will be needed to test if Landsat 8 multispectral and thermal analysis can confirm plume timing.

REFERENCES

ANDREWS, J.T., 1970, Differential Crustal Recovery and Glacial Chronolgy (6,700-0 BP) West Baffin Island, N.W.T.: Canada: Arctic and Alpine Research, v. 2, p. 115–134.

ANDREWS, J.T., 1987, The Late Wisconsin Glaciation and deglaciation of the Laurentide Ice Sheet, *in* The Geology of North America: North American and Adjacent Oceans During the Last Deglaciation: p. 13–32.

BLAKE, W., J., 1966, End Moraines and Deglaciation Chronology in Northern Canada, with special referece to Southern Baffin Island: Geological Survey of Canada, v. 66–22, p. 1–31.

BRODIE, J., SCHROEDER, T., ROHDE, K., FAITHFUL, J., MASTERS, B., DEKKER, A., BRANDO, V., and MAUGHAN, M., 2010, Dispersal of suspended sediments and nutrients in the Great Barrier Reef lagoon during river-discharge events: Conclusions from satellite remote sensing and concurrent flood-plume sampling: Marine and Freshwater Research, v. 61, p. 651–664, doi: 10.1071/MF08030.

CHIGBU, P., GORDON, S., and STRANGE, T., 2004, Influence of inter-annual variations in climatic factors on fecal coliform levels in Mississippi Sound: v. 38, p. 4341–4352, doi: 10.1016/j.watres.2004.08.019.

COLEMAN, J.M., ROBERTS, H.H., and BRYANT, W.R., 1991, Late Quaternary Sedimentation, *in* Salvador, A., ed., The Geology of North America: The Gulf of Mexico Basin: The Geological Socieity of America, p. 325–352.

DENTON, G.H., and TERENCE, J.H., 1981, The Last Great Ice Sheets: New York, *in* Mountain Research and Development: p. 484.

DOXARAN, D., FROIDEFOND, J.-M., and CASTAING, P., 2003, Remote-sensing reflectance of turbid sediment-dominated waters Reduction of sediment type variations and changing illumination conditions effects by use of reflectance ratios: Applied Optics, v. 42, p. 2623, doi: 10.1364/ao.42.002623.

ELEUTERIUS, C.K., 1978, Classification of Mississippi Sound as to Estuary Hydrological Type: Gulf Research Reports, v. 6, p. 185–187, doi: 10.18785/grr.0602.12.

FALCONER, G., and ANDREWS, J.T., 1969, Late glacial and postglacial history and emergence of the Ottawa Islands, Hudson Bay, N.W.T.; evidence on the deglaciation of Hudson Bay: Canadian Journal of Earth Sciences, v. 6, p. 1263–1276.

FALCONER, G., IVES, J.D., LOKE, O.H., and ANDREWS, J.T., 1965, Major end moraines in eastern and central arctic Canada: Geographical Bulletin, v. 7, p. 137–153.

LANE, R.R., DAY, J.W., KEMP, G.P., and DEMCHECK, D.K., 2001, The 1994 experimental opening of the Bonnet Carre Spillway to divert Mississippi River water into Lake Pontchartrain, Louisiana: Ecological Engineering, v. 17, p. 411–422, doi: 10.1016/S0925-8574(00)00170-1.

MICHELSON, D.M., CLAYTON, L., FULLERTON, D.S., and BORNS, H.W., J., 1983, The Late Wisconsin Glacial Record in the United States: Late Quaternary Environments of the United State: The Late Pleistocene, v. 1, p. 3–37.

OTVOS, E.G., 1984, Barrier Platforms; Northern Gulf of Mexico: Marine Geology, v. 63, p. 285–305.

PREST, V.., 1970, Quaternary Geology in Canada, in Douglas, R.J.,ed., *in* Geolgy and Economic Minerals in Canada: Ottawa Department of Energy, p. 676–764.

PREST, V.., 1984, The Late Wisconsin glacier complex: Geological Survey of Cananda Paper 84-10, p. 21–38.

SIKORA, W., and KJERFVE, B., 1985, Factors influencing the salinity regime of Lake Pontchartrain, Lousiana, a shallow coastal lagoon: Analysis of a long-term data set: Estuaries, v. 8, p. 170–180, doi: 10.2307/1351866.

APPENDIX

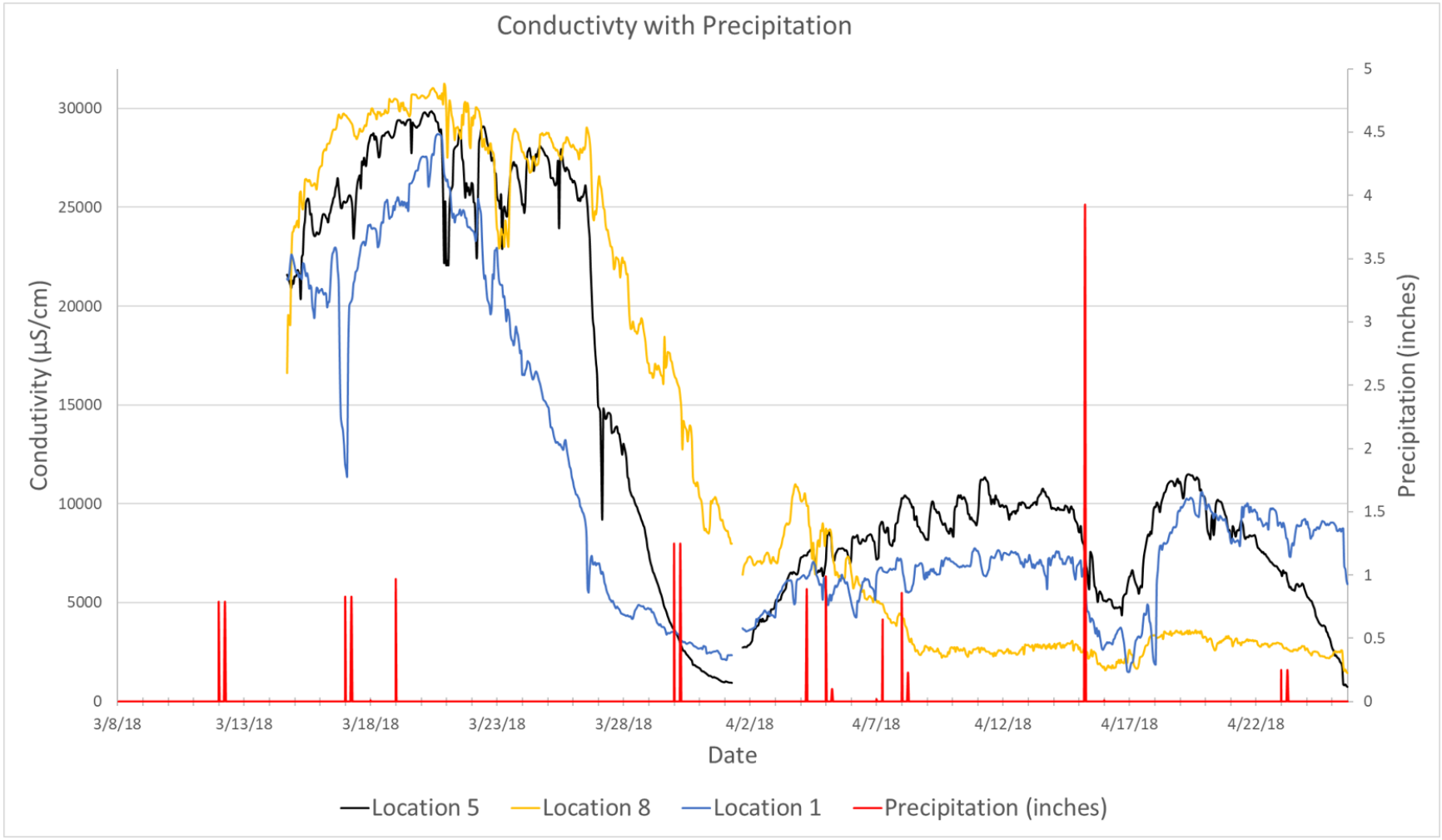

Figure 35a: Specific Conductance with Precipitation

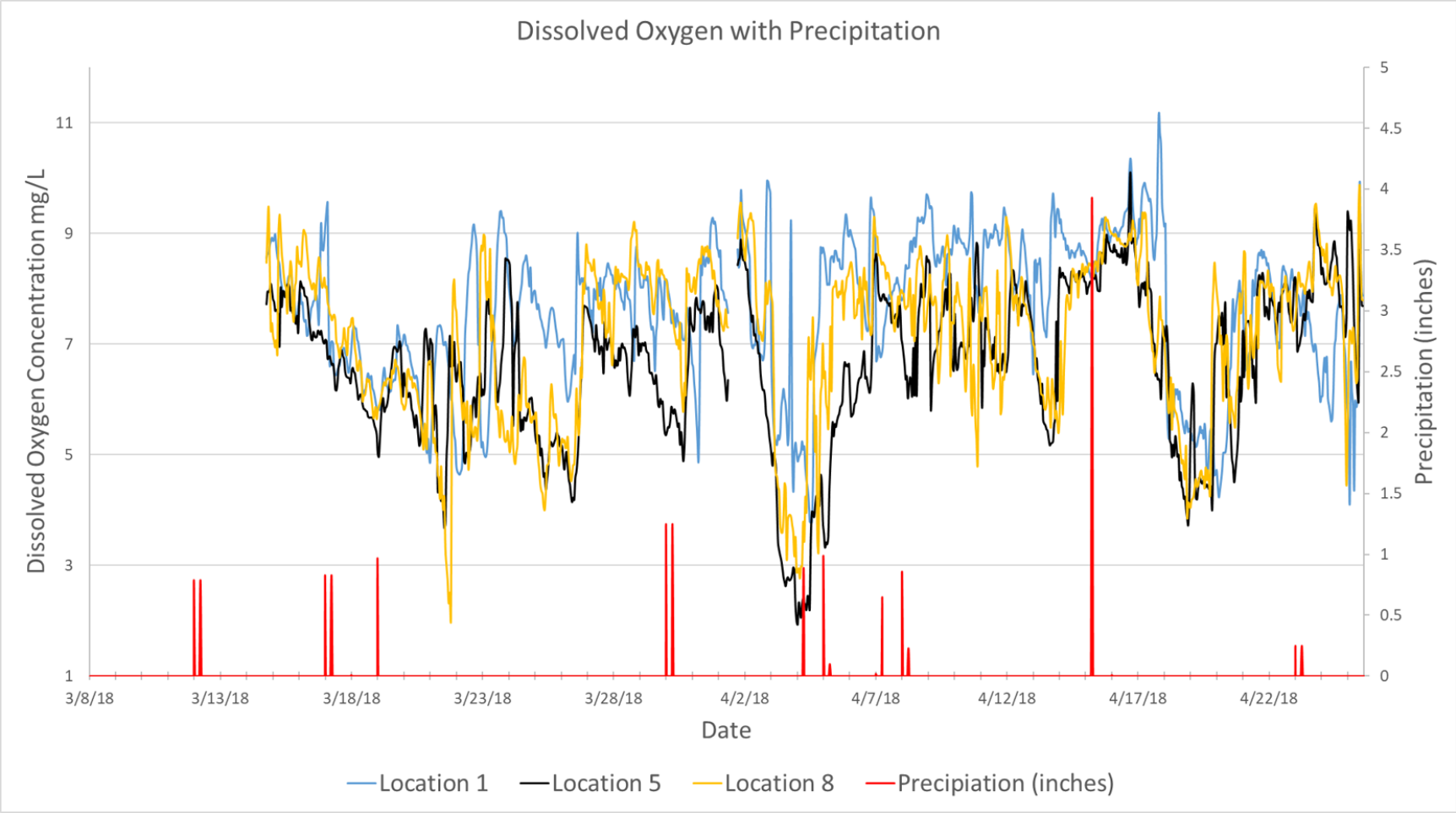

Figure 36a: Dissolved Oxygen with Precipitation

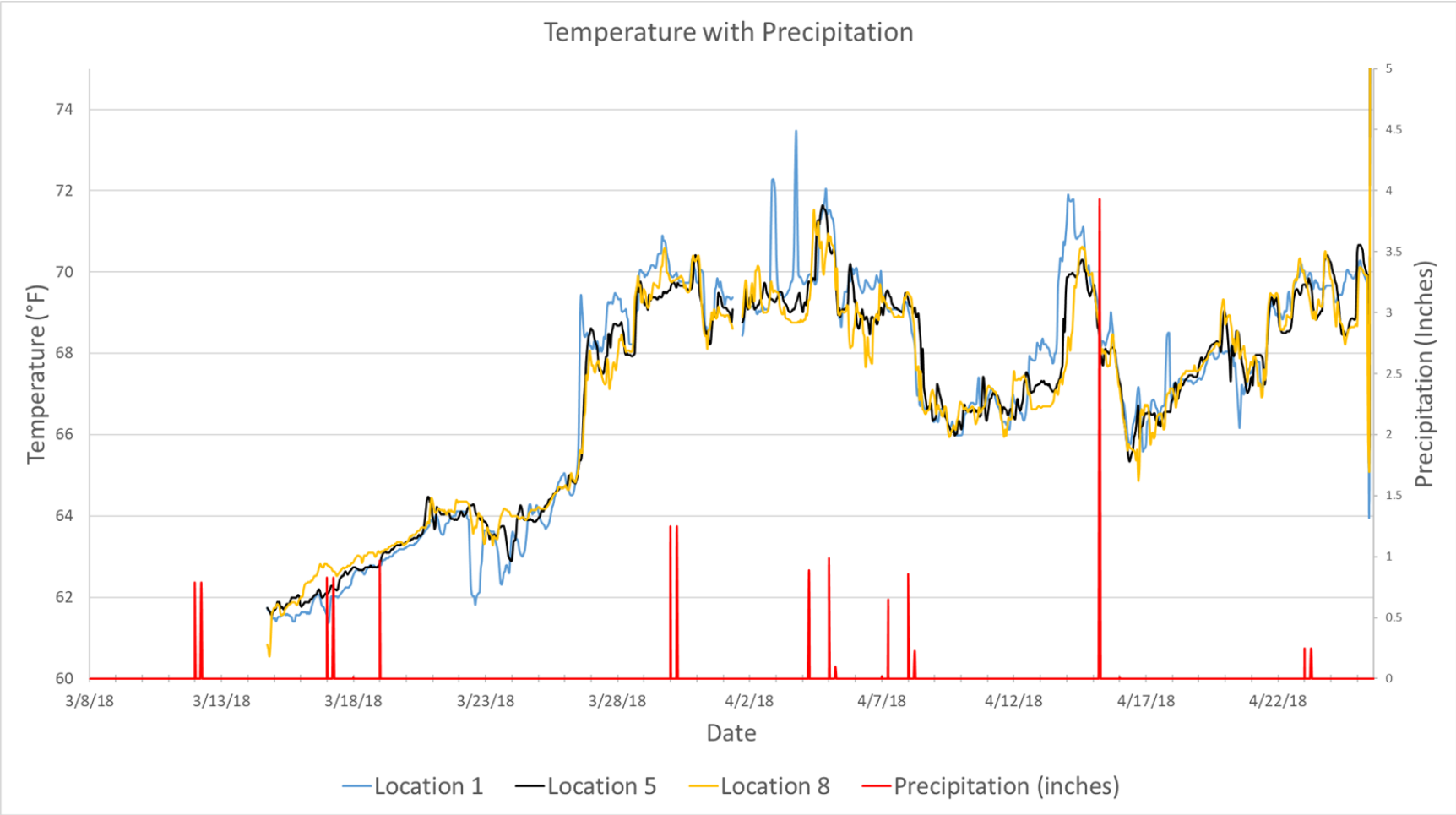

Figure 37a: Temperature with Precipitation

VITA

Jarett L. Bell was born and raised in Bay St. Louis, Mississippi. In May 2011, Jarett graduated from Bay High School and earned his Bachelor of Science in Geological Engineering from the University of Mississippi in University, Mississippi in May of 2017. In July 2017 Jarett decided to continue his education and was admitted to the University of Mississippi graduate school as a research assistant in the Mississippi Mineral Resources Institute where he would study under Dr. Greg Easson.

Jarett's work experience includes currently working as a full-time research assistant for the Mississippi Mineral Resources Institute as a graduate student after starting in July 2017. Work experience during his undergraduate degree includes: undergraduate teaching assistant for a non-major's physical geology lab from January 2017 – May 2017, and undergraduate research assistant for the Mississippi Mineral Resources Institute from August 2016 – May 2017.

Jarett's leadership, membership, and awards include: Association of Environmental and Engineering Geologists, The Society of Sigma Gamma Epsilon, where he served as president of both between 2016 – 2017; Phi Kappa Phi Honor Society; School of Engineering Graduate Achievement Award for Excellence in Academics, 2019.